Alma Mater Studiorum – Università di Bologna

DOTTORATO DI RICERCA IN

SCIENZE CHIRURGICHE

Ciclo XXXIII

Settore Concorsuale: 06/E1 – CHIRURGIA CARDIO-TORACO-VASCOLARE

Settore Scientifico Disciplinare: MED/22 – CHIRURGIA VASCOLARE

3D BIOPRINTING AND ITS APPLICATIONS IN VASCULAR SURGERY: IN-VITRO AND IN-VIVO TESTS FOR FUTURE 5D PERSONALISED NANOMEDICINE

Presentata da: Dott. Paolo Perini

Coordinatore Dottorato   **Supervisore**

Chiar.ma Prof.ssa Annalisa Patrizi   Chiar.mo Prof. Antonio Freyrie

Esame finale anno 2021

Index

Abstract

Three-dimensional printing techniques demonstrated the high potentiality of interactive processes applied to medicine and surgery. The current, wide availability of different materials and bio-inks allows the precise control of chemical and physical properties of the printed objects obtained through additive manufacturing technology. In addition, 3D printing may produce far-reaching changes in surgical pre-operative management, thanks to the potential interactions with medical imaging modalities.

We developed a method based on rapid freeze prototyping (RFP) 3D printer, reconstruction cutting, nano dry formulation, fast freeze gelation, disinfection and partial processes for the 3D to 5D digital models functionalization. We processed a computed tomography angiography scan of a human femoral artery bifurcation, and we reconstructed the 3D model of the vessel to obtain and verify the additive manufacturing processes. Afterwards, a biocompatible eluting-freeform coating for a drug-eluting balloon selected on the basis of the 3D-printed vessel was created under a biosafety cabinet. The alginate-printed coating contained 40nm fluorescent nanoparticles (NP), and was reconstructed by means of RFP printer, and gelled with ethanol (EtOH 98%). Feasibility and effectiveness of this 3D-printed scaffold was tested *in-vivo* and *in-vitro*.

In order to test this method *in-vivo*, the NP-loaded 5D device was deployed in a rat's vena cava. The coating dissolved in a few minutes releasing NP, which were rapidly absorbed in the vessel's wall, specifically interstitial tissue and vascular smooth muscle cells (confirmed with two-photon microscopy). NP internalisation was also confirmed *in-vitro*, on vascular smooth muscle cells, and on human umbilical vein endothelial cell (HUVEC) line.

We developed 5D, high-resolution, self-dissolving devices containing NP, which can be applied to the personalised medicine, specifically vascular and endovascular devices (such as coatings for drug-eluting balloons or stents, or vascular graft substitutes). In fact, NP can potentially be loaded with different drugs or molecules, in order to obtain a biological activity, thus clinical applicability.

Introduction

Chronic peripheral arterial disease (PAD) is the third leading cause of atherosclerotic cardiovascular morbidity, following coronary artery disease and stroke, and one of the principal causes of loss of walking ability. Currently, endovascular treatment (EVT) – mainly through balloon angioplasty (BA) – represents the most commonly performed treatment for patients affected by symptomatic PAD, followed by bypass surgery (BS)[1]. Over the last decades, important advances have been developed in endovascular technologies to address a great variety of anatomic challenges, and current and future efforts are directed toward improving long-term patency rates. Drug-coated balloons (DCB) are associated with lower rates of re-stenosis, thus a more durable benefit with less need of re-interventions[2]. However, BA and DCB are characterized by well-known limitations. In fact, only few different anti-proliferative agents (and excipients) are available, with fixed concentrations (thus limited device choice, and lack of personalisation).

The 3D printing techniques demonstrated the potential of interactive processes for medicine and its clinical applications, and related toxicity and vitality studies[3,4]. Materials selected for bio-printed scaffolds are predominantly based on both naturally developed polymers (such as gelatine, collagen, chitosan and hyaluronic acid) or synthetic molecules (e.g. polyethylene glycol)[5–7]. These molecules allow the accurate and specific management of chemical and physical properties[8].

5D-printing merges the data used to create 3D models with functionalization and customization (physiological activity); this process may lead to personalised therapy[9]. In this work, we describe how the 5D manufacturing method may be applied to create personalised models of patient's pathology[10]. Specifically, we investigated PAD and, in particular, the femoral artery bifurcation. We adopted the available 3D printing

technology to identify the best operative processes, and the related parameters, to obtain the optimal final object starting from a digital model. So, we selected bio-inks and new composite materials. Then, we customised macro- and micro-morphologies and biological properties (5D), merging these engineered devices with the shape obtained from the patient. Finally, in order to pave the way for future personalised medicine, we functionalised these printed object with nanoparticles (NP).

Current treatments for PAD

Medical Treatment. The aims of PAD treatments are: (i) symptoms resolution (or, at least, amelioration); (ii) improvement of patients' functional capacity; and (iii) reduction of cardiovascular and cerebrovascular morbidity and mortality, and slowing the progression of systemic atherosclerosis[11]. In general, oral antiplatelet therapy was found to be protective in terms of reduced risk of vascular occlusive events occurrence[12]. This includes patients with an acute or previous myocardial infarction or ischaemic stroke, angina (stable or unstable), PAD, or atrial fibrillation. Acetylsalicylic acid (ASA) is the most investigated antiplatelet agent, and long-term therapy is usually carried out with a low-dose oral intake of 75mg to 150mg daily. Daily ASA intake also demonstrated its effectiveness in terms of reduction of the risk of infra-inguinal bypass graft occlusion[13]. Clopidogrel 75mg daily has a comparable effect, demonstrating to reduce severe vascular events in a slightly larger portion of patients[12]. These results with clopidogrel were similar to those obtained with ticlopidine 250mg twice daily. Recently, the COMPASS trial proposed the combination of rivaroxaban 2.5mg twice daily (a Novel Oral AntiCoagulant, NOAC) and low-dose ASA for patients with lower extremity PAD[14]. This combination significantly reduced the incidence of major

adverse limb events and their related complications. Thus, this study concluded low-dose NOAC + ASA should be considered as an important therapy for patients with PAD[14]. Statin therapy has been shown to reduce cardiovascular events and mortality rates even in the most advanced stages of PAD, so it should be considered in all atherosclerotic patients[15–17]. Lifestyle modifications, such as stopping smoking, adopting a healthy diet, weight control, and regular exercise are particularly important in terms of life and limb salvage[18]. Finally, supervised exercise demonstrated its effectiveness in PAD patients, especially for those with intermittent claudication (IC)[19].

Surgical treatment. Surgical correction of PAD is indicated to obtain limb salvage and to resolve rest pain. In case of IC, it is usually indicated to start with medical treatment and supervised exercise[11,15,18,20,21]. The treatment choice should be based on patient's symptoms and his surgical risk, taking into account the anatomical distribution of the atherosclerosis[22]. Surgical treatment mainly consists in BS or endarterectomy (EA). BS redirects the blood flow around an arterial occlusion or stenosis, in order to increase the distal perfusion of the limb. BS can be classified in anatomic or extra-anatomic. While an anatomic bypass (e.g. femoro-popliteal bypass) follows the normal vascular pathways, an extra-anatomic bypass (e.g. axillo-femoral bypass) is placed outside a normal path but still represents an important tool for vascular surgeons. BS can also be classified according to the grafted material: autologous (e.g. great saphenous vein, femoral vein, upper limb veins), prosthetic (polytetrafluoroethylene, PTFE or polyethylene terephthalate, Dacron), or allografts (e.g. cryo-preserved arterial or venous homografts). Autologous material is associated with better patency rates (77.2% for above-knee vein, 64.8% for below-knee vein at 5 years)[23]. The early mortality rate is usually below 2%, mostly due to heart complications[18,23].

EA is a basic vascular procedure, which involves the removal of obstructive or stenotic atherosclerotic plaque from the arterial lumen. EA can be performed as the sole therapeutic technique, or in combination with BS. Several methods for EA are described in literature, including: open EA, semi-closed, or eversion EA. Regarding open EA, the artery is usually opened through a longitudinal arteriotomy. The plaque is then removed, following a plane developed between the atherosclerotic plaque and the media or adventitia. The arteriotomy is eventually closed primarily, or with a patch (prosthetic, autologous vein, or heterologous patch such as bovine pericardial patch)[24].

Finally, all surgical "open" treatments can also be combined with EVT, in order to perform a hybrid treatment[25].

Endovascular treatment. Thanks to recent advances in endovascular materials and techniques, catheter-based intervention represents now a feasible and widespread treatment modality for PAD, and percutaneous treatments regularly replaced standard open surgery as the first line treatment. An EVT is often the default strategy, especially for short stenosis or occlusion of the iliac arteries. In fact, in this case, long-term patency is excellent (more than 90% after 5 years of follow-up), with low risk or complications[26]. EVT advantages include: avoidance of general anaesthesia, avoidance of incision-related complications, reduced cardiovascular stress, and faster recovery. Even though EVT is associated with higher rates of restenosis or re-occlusions, re-interventions are more easily performed when required[11,24,27]. EVT for PAD include the following techniques: percutaneous BA, stenting, endografting (by using covered stents). Additional techniques and devices include: DCB, drug-eluting stents, atherectomy (excisional or ablative), thrombectomy, and thrombolysis[28–31]. In general, the approach to PAD patients should be planned based upon the location of the arterial lesion, its suitability for BA or BS, patient's surgical risk, and patient's life expectancy.

Finally, the possibility that a specific EVT may limit future surgical options should be considered.

History of 3D-bioprinting

The addictive manufacturing industry was revolutionised in the eighties. An American engineer, Charles Hull, built the first 3D printer. Basing on an object created with computer-aided design (CAD), this printer was able to depose sequential layers of an acrylic photopolymer, which was concurrently cross-linked by UV light, creating a solid 3D object. This technology was named stereolithography (STL)[32]. Then, in the nineties, healthcare professionals started to 3D-print dental implants, custom prosthetics and kidney bladders. Afterwards, the term "3D-bioprinting" started to appear in literature. "3D-bioprinting" was adopted when the material being printed, so-called "bio-ink", was made of living cells, biomaterials, or active biomolecules[33]. 3D-bioprinting, similarly to additive manufacturing, consists in layer-by-layer deposition of bio-ink for 3D tissues and organs creation[32–34]. In addition to organ and tissue printing, 3D-bioprinting can also be employed for tissue models fabrication, disease modelling, and numerous other *in-vitro* applications.

Currently, 3D-bioprinting may be classified in three sub-groups: extrusion, droplet, or laser-based bioprinting[32,34,35]. Each bio-printing modality has its own bio-ink selection, based on bio-ink's viscosity, rheology, cross-linking chemistry, and biocompatibility. Over the last decades, bio-inks evolved, as well as secondary techniques to overcome 3D-bioprinting limitations. For example, low-viscosity bio-inks may be extruded in a granular support bath containing yield stress hydrogels which solidify around the printed structure in order to prevent its collapse[36]. In the meantime, significant advancements were also obtained in imaging modalities, and post-processing

software programs. Nowadays, thanks to the above-mentioned progresses, 3D bio-printing is emerging as a encouraging new approach for the fabrication of complex biological creations in the fields of tissue engineering, regenerative medicine and reconstructive surgery[32].

In the current work, we applied these techniques, specifically 5D additive manufacturing, to create personalised models of patients' pathology, and to pave the way for the future creation of personalised, active coatings for DCB, or vascular graft substitutes.

Materials and Methods

Computed Tomography

To 3D-print a femoral bifurcation, we started from a Computed Tomography (CT) Angiography (CTA) of a PAD patient. All CTA were performed with a 128-section CT system (SOMATOM Definition Flash, Siemens Healthcare GmbH, Erlangen, Germany).

A standard lower extremity CTA was carried out in cranio-caudal direction during deep-inspiration breath-hold, with scan volume from the para-renal aorta to the feet, and consisted in a two-phase acquisition. A first, unenhanced, phase to clearly identify the presence of calcifications or previously implanted materials such as vascular stents, was followed by an arterial phase with bolus tracking. Contrast medium was injected through an 18-gauge cannula in an antecubital vein with the use of a double-syringe electronic injector (Medrad Stellant, Bayer HealthCare LLC, Whippany, NJ, USA). Initially, 60 mL of a non-ionic, monomeric iodinated contrast medium (Iomeron 400, Bracco SA, Milan, Italy) was administered at a rate of 3 mL/s, followed by 30 mL at 2 mL/s. Finally, a 40-mL saline chaser was injected at a 3mL/s rate. A region of interest (ROI) at the level of the aortic bifurcation was used for bolus-tracking; the scan started 15 s after the enhancement of this ROI crosses the threshold trigger of 140 Hounsfield Units (HU). Additional data acquisition parameters were: voltage 120-140 kV, current 200-250 mAs, pitch 1.0, collimation 128x0.6 mm, and rotation time 0.5 s. CTA were reconstructed at 1-mm slice thickness, every 0.7-mm slice increment.

3D printable model creation

Images were exported in Digital Imaging and Communications in Medicine (DICOM) format, then uploaded and analysed on an independent dedicated workstation equipped with an open source medical image viewer (Horos 2.4.0, The Horos Project). First, the CTA-scan was viewed in 3D-Volume Rendering (3D-VR) modality. Bones were removed with the appropriate tool. Residual fragments, or structures, other than arteries, were removed with the scissor tool. Then, the CT-scan was cropped by leaving only that area of interest (i.e. the femoral bifurcation), in order to obtain a smaller STL file.

Multiple ROI were placed along the course of the arteries to obtain Hounsfield numbers of the vessels of interest. Then, a new, separate series based upon these HU intervals was created.

Finally, the 3D Surface Rendering can be created, and the 3D model exported to an STL file for 3D printing. Since some surface details of this STL model may be not printable, the STL file usually needs post-processing with a CAD-like software.

Our 3D-printing lab is equipped with: custom-made hybrid printer, hybrid deposition printer in climatic chamber, stereolithography printer for resins polymerization, custom-made rapid freeze prototyping printer, and 6 laboratories for rapid prototyping.

General equipment description

Most of the tests regarding *in-vitro* and *in-vivo* studies, as well as simulation tests, were carried out in the Laboratories of the Department of Medicine and Surgery,

University of Parma, and in the Common Research Centre of the University Hospital of Parma. The Common Research Center of the University Hospital of Parma consists of about 1600 square meters of research space, made up of various, closely linked components. The research/diagnostic laboratory (CoreLAB) with genomic, proteomic and cell biology facilities, contains the following technologies/expertise: micro array (Affimetrix and Agilent platforms), nucleic acid extractors (Hamilton MicroLab STARlet), flow cytometry and cell sorting (FACS Aria III, Becton-Dickinson; F500, Beckman-Coulter), bioinformatics.

The SIM.LAB (Clinical Simulation Laboratory) of the University of Parma, located within the Hospital area, provides a space already suitable for simulation and training for a wide range of clinical and surgical procedures, and was used for preoperative EVT planning and material selection. The SIM.LAB consists of about 300 square meters of simulation space, and includes: one operating theater simulation room (with the possibility to use fluoroscopy with a mobile C-arm), an endoscopy simulation room (gastrointestinal and bronchial), a surgical hand scrub simulation space, two rooms dedicated to control/direction and filming (equipped with ETC FusionHD FULL KbPort), a storage area, a skill room (to train skills such as peripheral or central venous catheter insertion, arterial cannulation, vascular accesses, or cardiopulmonary resuscitation) divided into three compartments, a medical office for communication laboratory, offices for secretaries and technical services. In particular, the operating theater simulation room is equipped with different manikins, a virtual patient simulator and skill trainers related to different medical specialties.

3D bio-printer settings and analysis, and model design

Part of the materials and methods described in this section was also preliminarily published in a peer-reviewed scientific journal[10]. The rapid freeze prototyping bio-printer was custom-made (Arduino-based). It was positioned under a biosafety cabinet (HeraSAFE Heraeus, Thermo Fisher Scientific, Waltham, MA, USA), and equipped with 2 mechanical extruders for 5ml syringes (BD Emerald, Franklin Lakes, NJ, USA), and a removable Peltier cold plate[34]. The cold plate temperature was measured with a Flir A325 infrared camera (Flir Systems, Wilsonville, OR, USA). Then, a scaffold was designed, getting the following characteristics: biocompatibility, ability to dissolve itself, capability to be functionalized by NP addition. The scaffold was designed using SolidWorks2015 (Solidsolution, London, UK), and sliced with Slic3r open source software (Slic3r 1.3.0, www.slic3r.org).

Development of the nano-functional scaffold

In order to develop the scaffold/coating, we used two different materials as bio-inks: alginate powder and natural polylactic acid (PLA), as previously described in our recent publication[10]. The first one, alginate powder (W201502, Sigma-Aldrich, Steinheim am Albuch, Germany), is a low-cost hydro-soluble biomaterial used for sweets fabrication or for molecular cooking. The second one, natural PLA (175N1, Velleman Inc., Legen Heirweg, Gavere, Belgium) without colour pigments (diameter 1.75mm, density $1.25g/cm^3$ (at 21.5°C), printing temperature 190-225°C, impact strength $5kJ/m^2$), recently demonstrated its use for clinical applications[8,37].

Nano Dry Formulation (NDF). To minimize particle aggregation, all NP (40nm Fluorescent nanobeads, Thermofisher, Milano, Italy) were sonicated (Branson Ultrasonics, Danbury, CT, USA) for 30 minutes at T=37°C, and 3μl (50μg/ml) of NP solution were added into sodium alginate powder. This sonication was performed before all the following experiments involving NP. Afterwards, high-glucose Dulbecco's Modified Eagle's Medium (DMEM) without phenol red (Gibco, Thermo Fisher Scientific, Waltham, MA, USA) was added, in order to achieve a final alginate solution concentration of 7%, 9% and 11% wt/vol.

3D Fast Freeze Gelation (3DFFG). Scaffolds were printed onto aluminium plate with a temperature of about -30°C (at room temperature), through a 26G needle (BD Emerald, Franklin Lakes, NJ, USA), and covered with ethanol 95% in order to obtain gelation and disinfection, simultaneously[38,39]. Specifically, the nano-laden scaffolds that will be used for the following *in-vitro* and *in-vivo* tests were 3D-printed with alginate 11% at 6mm/s printing speed. These printing values were in accordance with the under-mentioned results of the macro-morphological characterisation and resolution assessment.

Characterisation of the coating micro-porosity

Scanning electron microscopy (SEM) characterizations of the 3D-printed scaffolds were performed using a field emission SEM (FESEM, Nova NanoSEM 450, FEI company, Hillsboro, OR, USA). This was useful to obtain morphological information, specifically micro-porosity characterizations, of the 3D-printed objects. All-images were acquired in field-free lens mode using the Everhart-Thornley detector

for the secondary electron imaging signal. The accelerating voltage of 10kV, the spot size of 4.5nm, and the working distance of 6mm were used for all image acquisition[10].

In-vitro vascular smooth muscle cells (VSMC) tests

Cell culture. Part of the following methods was recently, preliminarily published in literature by our research group[10]. Mice VSMC were cultured in DMEM (high-glucose) with 2mM glutamine, 10% foetal bovine serum (FBS, Euroclone, Milano, Italy) and 1% penicillin/streptomycin (5,000 UI/mL). Cells were cultured as recommended and maintained under standard cell culture conditions at 37°C in a water-saturated atmosphere of 5% CO_2 in air. We seeded 3×10^5 VSMC in a 50mm Petri dish for direct and indirect measurements, for a total of eight measurements. Regarding the direct measurement, we added after 24 hours the alginate scaffold-enriched NP (50μg/ml) cross-linked with ethanol to the culture, as described above. For the indirect method, the same scaffold-enriched NP was totally dissolved directly in the medium before being added to the culture.

Viability assay. In order to evaluate cell viability, VSMC were counted in a Buerker haemocytometer by trypan blue exclusion method and evaluated under a phase contrast microscope. Cell viability was also confirmed using calcein acetoxymethyl (AM) staining (Thermo Fisher, Waltham, MA, USA). Specifically, after the treatment, the media was replaced with a fresh one containing 5μM calcein AM. After 30 minutes of incubation at 37°C in 5% of CO_2, cells were washed twice with phosphate buffered saline (PBS) before being imaged with an upright fluorescent microscope (Leica Microsystems, Wetzlar, Germany) through a x20/0.7 or x40/1.3 oil objective.

Scaffold dissolving methods. We performed two different dissolving methods:

15

1. Direct method: the scaffold was placed directly in the Petri dish containing cells with 4mL of culture medium;

2. Indirect method: the scaffold was placed and dissolved in a 15mL tube into 2mL of culture medium. Once the scaffold was dissolved, we added 2mL more of culture medium; then, this solution was added in the Petri dish, where the cells were previously cultured.

In-vivo experiments

We tested a total of five Sprague Dawley rats. Preliminary results on two albino laboratory rats were already published by our research group, using similar methods[10]. These experiments were performed in accordance with the local ethical guidelines. The protocol was approved by the Italian Ministry of Health (Prot. N 989/2017.PR). All the procedures followed the directives of the European Law 63/2010 and the Italian law 26/2014 for experimental animal use. Animals were anesthetised, and the inferior vena cava was exposed through surgery[39]. The proximal portion of the inferior vena cava was ligated, and the NP-laden scaffold was inserted 1cm distally, via a 26G needle through a short venotomy. This scaffold was left in place for 2 minutes in the vena cava, in order to obtain complete dissolution. Then, the vessel was removed. This specimen was subsequently washed in PBS, opened with a longitudinal venotomy, and fixed in 4% buffered formalin solution for 24–48 hours before two-photon microscopy evaluation.

Microscope analysis for *in-vitro* and *in-vivo* tests

Parts of the following materials and analyses were preliminarily published in literature by our research group[10].

Stimulation-emission depletion (STED) microscopy. Before STED microscopy analysis, the cells were fixed on a cover glass (thickness n°1.5) with 4% paraformaldehyde (PFA) for 10 minutes; then blocked, and permeabilised with 3% normal goat serum, 0.1% Triton X-100 in 1 x PBS for 1 hour as previously described[40]. Briefly, STED xyz images were acquired with a Leica SP8 STED3X confocal microscope system (Leica Microsystem, Wetzlar, Germany). Green NP (Molecular Probes, Eugene, OR, USA) were excited with a 488 nm Argon Laser, and emission was collected from 507 to 614nm, while wheat germ agglutinin (WGA, Thermo Fisher, Waltham, MA, USA) was excited with a 545/547nm-tuned white light laser (WLL), and emission was collected from 555 to 647nm. Sequential acquisition was applied to avoid fluorescence overlap. A 660nm conventional wisdom (CW)-depletion laser was used for both excitations. Images were acquired with a Leica HC PL APO 100x/1.40 oil STED White objective. CW-STED and gated-STED were applied to the fluorescent NP and WGA, respectively. Collected images were de-convolved with Huygens Professional software (Scientific Volume Imaging, Hilversum, The Netherlands) and analysed using Imaris 7.4.2 software (Bitplane, Belfast, UK).

Two-photon microscopy. The laboratory rat's vena cava exposed to NP-laden scaffolds was fixed and stained with WGA, and imaged with the two-photon microscopy (Trim Scope II, LaVision BioTec, Bielefeld, Germany). Two-photon microscopy allows cells and NP imaging for the entire thickness with a 10–20 μm of Z-stack[40].

In-vitro human umbilical vein endothelial cell (HUVEC) analysis

The sterile plastic material for the cell cultures was purchased from Costar, Corning (Amsterdam, The Netherlands), and PBS from Euroclone (Milano, Italy). The ATP colorimetric assay kit was obtained from Novus Biologicals (Centennial, CO, USA). MTT (3-(4,5-dimethyl-thiazol-2-yl)2,5-diphenyl tetrazolium bromide) was provided by Sigma (St. Louis, MO, USA), which also supplied all of the other reagents, unless otherwise specified. Regarding HUVEC analysis, parts of the materials and methods described below were preliminarily published in literature by our research group[10].

Cell culture, treatment and proliferation/viability studies. HUVEC (purchased from Lonza, Basel, Switzerland) were grown in a fully supplemented EGM-2MV Bullet Kit (Lonza, Basel, Switzerland) at 37°C in a 5% CO_2 humidified incubator. Before the treatments, cells were seeded in plates and cultured to 80-90% confluence.

Next, we seeded $3x10^5$ HUVEC in 2mL of medium for 2-24-48 hours before toxicology assays, applying both the direct and the indirect treatment previously described for the VSMC.

Cells' morphology was monitored using an inverted microscope (Olympus CK40-RFL, Tokyo, Japan), and their number was evaluated by cell counting in a Buerker haemocytometer.

Viability was also assessed by MTT assay. The formazan crystals were solubilised, and the absorbance was measured using an automated microwell plate reader (Multiskan Ascent, Thermo Labsystems, Helsinki, Finland) at 550nm.

Cellular ATP levels were determined using the ATP assay kit, following the manufacturer's instructions. All results were expressed as the percentage of controls

(untreated cells). The uptake of fluorescent NP was evaluated by flow cytometry using a FC500 flow cytometer (Instrumentation Laboratory, Bedford, MA, USA). Data were processed using the FlowJo software package (Tree Star Inc., Ashland, OR, USA).

Statistics

Normal distribution vs. skewed distribution of variables was assessed with the Kolmogorov-Smirnov test. Statistics of variables included One-sample T-test signed rank test, unpaired Student's t-test, two-way ANOVA (post hoc analyses: Bonferroni test or Games-Howell test, where appropriate), Wilcoxon sign rank test and Kruskal-Wallis (post hoc analyses: Dunn's multiple comparison). Data were analysed with Epi Info 7.2.2.16 (CDC, Atlanta, Ga, USA), or Prism 6.0 software (GraphPad Software, San Diego, CA, USA). Details about the specific test adopted for each experiment will be described in the figure legends. A p value <.05 was considered statistically significant.

Results

The 5D printing technique is the result of data regarding 3D printing technologies merged with local control composition of the biomimetic materials (+1D), and particles distributions with the capability to reproduce a life-like organ response during physiology studies (+1D)[9,41]. Starting from a patient's CTA, we continued by reconstructing the 3D model of his femoral artery bifurcation. Then, we obtained a nano-laden aerogel as a carrier for the fast release of integrated NP. These bio-printed devices were subsequently used to realise a biomimetic bio-composite material (4D) for the *in-vitro* and *in-vivo* tests. Eventually, we customised the 4D model by adding NP, which directly interacted with the organ physiology, obtaining a 5D bio-printed device.

The design of a standardised approach, to develop 5D printed devices, required 3 phases (Table I): pre-printing, printing and post-printing[42]. Each phase requires the analysis and the validation of the following modelling steps: (i) requirement; (ii) model orientation; (iii) trajectory generation; (iv) printing process analysis; and (v) digital model adherence[10].

Using a Peltier-based system (Fig. 1a), we developed soft scaffolds (Fig. 1b) with a complex shape (Fig. 1c). The implemented cooled bed (Fig. 1d) reached a temperature of -30°C in 19.6±0.9s (31.2±0.1°C in 120s), and returned to room temperature ($\Delta T=57$°C) in 25.4±0.7s.

The selected mechanical micro-extrusion technology, with volumetric planning, did not require any process change in the use of different materials or bio-ink viscosities (Fig. 2a)[10,43]. Real-time pressure adaptation is necessary, since this would be impossible by pneumatic control extrusion alone (Fig. 2b-d). To obtain dimensions very close to those of a 26G syringe needle (inner diameter $\Phi = 292\mu m$), we found that by using a concentration of 11% alginate the fresh filament diameter, measured after 3D printing,

was the optimal biomaterial concentration (Fig. 3a, green columns). On the other hand, when using 7% and 9% alginate solutions for scaffold fabrication with 400μm of macro-porosity, it was difficult to preserve the bridge for the required freezing time. Thus, it was required a low environmental temperature to subtract the thermal energy in a shorter time. Or, to maintain the same speed, we had to print a larger filament to adequately distribute the filament weight, which would not fit the 26G needle. The minimum deposition speeds for the different percentages of biomaterials to maintain a regular shape distribution were: 6 mm/s for 11% of alginate (Fig. 3b); 10 mm/s for 9% of alginate (Fig. 3c); and 14 mm/s for 7% of alginate (Fig. 3d). Eventually, with the minimum speed (6 mm/s) and maximum concentration (11% of alginate) we used for 3D bio-printing, we also performed a validation test of both corners and drop (Fig. 3e, 3f), proving the high resolution of the applied technology. Parts of these results were preliminarily published in literature in a peer-reviewed journal paper[10].

We developed the creation of models of fast release vascular therapy through the bio-printing fixation (Fig. 4a), followed by freeze gelation, using ethanol (Fig. 4b), allowing the fabrication of 5D nano-laden hydrogels (Fig. 4c)[44]. We initially printed a total of eight scaffolds, with and without 40nm fluorescent NP addition (Fig. 4d). These scaffolds self-dissolved in DMEM in 198.3±1.6s, and 207.3±2s, respectively. The difference of dissolution time between the two groups (with or without embedded NP) was not statistically significant (Fig. 4d). On the other hand, the normal $CaCl_2$ gelation scaffold (Fig. 4e) displayed the same structure after 24 hours. The alginate-printed scaffolds showed an extremely porous and fibrillar microstructure, as depicted by scanning electron microscopy (SEM) images. The high surface area led to a greater interaction with biological tissues (Fig. 4f). Conversely, ethanol-gelled structures (Fig.

4g) presented a more compact and less porous microstructure, characterised by a higher speed of resorption, release of drugs, and reduced surface volume ratio[10].

Preliminary *in-vitro* analysis on VSMC (Fig. 5), demonstrated cell viability in both the considered gelation processes ($CaCl_2$ and ethanol). Dissolution time for both direct and indirect methods was similar, and the difference was not statistically significant if compared to control.

Then, after the dissolution of these bio-printed structures (Fig. 6a), NP internalisation into VSMC was revealed through STED confocal microscopy (Fig. 6b-d). Subsequently, we inserted the same NP-laden structures in a rat's vena cava (Fig. 7), in order to confirm the feasibility of these methods *in-vivo*. Dissolution occurred in a short amount of time (approximately 2 minutes)[10]. We confirmed NP internalisation into both the interstitial tissue and the vascular cells (Fig. 6e-g)[45]. To corroborate our findings, during the last year of this project, we repeated the *in-vivo* experiment with four additional albino laboratory rats. We obtained similar results even if we modified the technique. In fact, the scaffold dissolved in approximately 2 minutes also in the rat's aorta, and in a non-ligated vena cava. Finally, NP internalisation was confirmed via two-photon microscopy.

Eventually, cellular vitality and metabolism were assessed in a HUVEC line, to test if our printing method may alter cell surviving in any way. The percentage of alginate (11%) we used for our biological application did not influence cellular vitality or metabolism in both direct (Fig. 8a, c, e) and indirect (Fig. 8b, d, f) methods for dissolution. Likewise, gelation and NP administration did not alter the HUVEC viability or metabolism (Fig. 8a-f). To check if NP may interact with our cell line, we also performed a cytofluorimetric analysis, which demonstrated HUVEC can bind and/or internalise NP with slight 24 hours changes (Fig. 8g).

22

Basing on these preliminary results from *in-vitro* and *in-vivo* studies, we moved on from functionalization method (4D), to customisation method (5D). So, we printed a model of a femoral artery bifurcation (Fig. 9), directly from a patient's CT-scan with the aim to reconstruct, by 3D bio-printing, the portion of interest (Fig. 10) with sodium alginate-based material. The bio-ink was functionalised with an interface and the relative reinforcement, obtaining a composite biomaterial (Fig. 11a). Basing on this result, we manufactured a bio-composite material (nano-functionalised 4D bio-engineered scaffold) with a new type of fibre (Fig. 11b), customised with different functional matrix (for cellular adhesion, gradual release, etc.) (Fig. 11c). Finally, we merged this material with the correct technology parameterisation, and we printed and perfused a complex vessel system (Fig. 11d–f).

The fibre (Fig. 11g) allowed scaffold engineering (performance mimicry, vascularisation for cell viability). The surface micro-morphology modification (Fig. 11h) enabled different types of applications (cell adherence, active or passive stimuli response). With different types of coating and matrix we could customise the 4D bio-composite materials (Fig. 11i)[10]. Also, in order to print the nano-laden scaffold, we could realise a composite biomaterial, or rehydrating an aerogel scaffold. Then, after the implementation of the adhesive coating and matrix, we could customise the biological device (Fig. 11j) to achieve the desired physiological properties (Fig. 11k).

Finally, we obtained a 5D bio-printed device as a theoretical, customised coating for a DCB for percutaneous angioplasty (Fig. 12a–d)[9]. The reported fabrication processes pave the way for the post-printing phases, and "6D" smart material device (e.g. autonomous regeneration). These next phases will include tissue and organ reconstruction, medical training on bio-printed objects (Fig. 12e–g), and/or systems for

the controlled release for scaffold functionalization (e.g. vascularised scaffold, capillary systems) (Fig. 12h).

Discussion

The worldwide prevalence of PAD is uncertain[46]. Nevertheless, approximately 8 to 10 million people are affected with lower extremity PAD in the United States, and almost 40 million in Europe[15,20]. Moreover, the number of patients with PAD is rising, due to global aging, growing world population, and increased incidence of diabetes and hypertension.

Even though PAD may be asymptomatic in more than 20% of the cases, typical clinical manifestations include some type of pain[47]. Atherosclerotic stenoses or occlusions within the lower extremity arterial tree reduce the blood flow to the leg, causing varying degrees of soft tissue ischemia. Symptomatic PAD may present as IC, or with limb-threatening ischemia associated with rest pain and/or ischemic ulcerations or gangrene, usually referred to as chronic limb-threatening ischemia (CLTI)[18]. Unlike IC, which rarely progresses to the point of requiring amputation, CLTI is associated with a high risk of limb loss without intervention[21].

The BASIL (Bypass Versus Angioplasty for Severe Ischemia of the Leg) trial, is the only multicentre, randomized controlled trial (RCT) which compared BS and EVT/BA[1]. This study concluded that these two treatments are associated with comparable outcomes in terms of amputation-free survival. Each strategy demonstrated its own different advantages and drawbacks. In fact, patients who underwent BS experienced a more durable benefit, but this approach was associated with a significant higher rate of post-operative morbidity, greater length of stay, and more frequent need of intensive-care unit stay. On the other hand, the BA group experienced lesser early morbidity rates and shorter length of stay, but higher immediate failure and 12-month re-intervention rates. Finally, average costs were lower in the latter group.

One of the major limits of this RCT, is that current endovascular technologies have not been included[27]. In fact, due to its clear advantages at least in the short-term, EVT represents – at present – the most commonly used treatment for PAD[48].

DCB are made up of a semi-compliant or non-compliant balloon catheter covered with an anti-proliferative agent (typically paclitaxel), and an excipient (e.g. urea) to facilitate drug transfer into the vessel wall on balloon inflation[2]. The main advantage provided by DCB angioplasty over plain old BA (POBA) is the lower rates of re-stenosis, thus a more durable benefit with less need of re-interventions. In fact, POBA has been associated with 1-year re-stenosis rates up to 60% in the femoropopliteal region[2,49]. Even though the implantation of a bare metal stent (BMS) may halve the risk of re-stenosis, BMS are associated with additional complications such as fractures, thrombosis and in-stent re-stenosis[2,48,50]. Recent RCT reported favourable outcomes with DCB when compared with POBA. One-year primary patency rates were 87.5% in the IN.PACT SFA, 82.3% in the ILLUMENATE US, and 73.5% in LEVANT 2[2,51,52]. Significantly higher primary patency rates were confirmed at 36 months follow-up (69.5% in the DCB group vs. 45.1% in the POBA group; log-rank P<.001)[2]. To note, these results were similar to those obtained with drug-eluting stents[53]. At present, new, customizable, endovascular devices are eagerly awaited, in order to improve target lesion patency and extend EVT feasibility.

The production of synthetic organs and living tissues requires the realisation of bio-mimetic bio-scaffolds for cell seeding, the presence of integrated vascular systems for long-term perfusion, and a precise cell deposition process with the related scaffold customisation for 5D technique implementation and bio-mimicry screening[8,10]. The macro-structure should allow the synthetic organ function bio-mimicry (e.g.

vasoconstriction), while the surface characteristics should support cell adherence and subsequent cell vitality.

Using the Formulation and Analysis for Nanoparticle Additive Manufacturing (FANNAM) method (Table I) applied to the reconstruction of PAD, it is possible to carry out pre-surgical training and 5D short-term medical device, identifying the correlation and the related scheduling between methods steps, parameters, operative processes, and the printing phases related to organ printing[10,34,42,54]. The realisation of 5D printed soft tissues (cf. Table I) requires: (i) evaluation of the parameters resuming the interaction between the 3D printed object and the selected biological tissue; (ii) functionalization to apply operative processes in health application; and (iii) validation of the printing phases with 3D partial processes and customisation of digital bio-library. The 3D pre-printing process requires three major steps: (i) image acquisition and selection, slicing and analysis; (ii) computer aided tissue engineering (CATE) processing; and (iii) printing. The first step, i.e. image acquisition, is achieved with Magnetic Resonance Imaging or CT; CT is usually the preferred method by reason of its faster sampling. Volumetric data are rendered in DICOM format, which cannot be directly 3D printed[55]. Thus, image data require conversion to .STL format, using a specific software; then, the g-code generated by computer aided manufacturing (CAM) controls the motors[56]. The selected material and its customisation address the selection of technology and the correct printing parameters for its manipulation. The total quality improvement process begins by recognizing the type of object and the quality evaluation of the results for the adopted production technology and concerns: material properties, geometric parameters, micro-porosity, the degradation of the gelled object, as well as the cells' viability and/or the material toxicity[10]. RFP technology allows the high-defined scaffolds development. Thus, the method we are presenting may improve

the current state of the art[57,58]. Indeed, we were able to obtain the same resolution of the existing technology, while avoiding the use of toxic photo-activators, indispensable for the stereolithographic apparatus (SLA)[10,59]. Additionally, in contrast to selective laser sintering or SLA, we did not produce material waste. Furthermore, the use of cell-laden bio-ink would not be possible with standard fused deposition modelling, since it passes the temperature of 37 °C.

High resolution was achieved by identifying 46 geometrical parameters for the scaffold analysis, developing a continuous improvement operative process to better understand and validate the deviation trend and applying the inner diameter value as "filament parameter"[8,10,58]. Difficulties regarding the height of the layer were solved, and variance using the geometrical parameters was reduced as well as the incomplete lap, the over accumulation and the redundant lap[57,60]. In this context, viscosity has a key role in the deposition of filament without support (bridge). As a matter of fact, it is well known that alginate dissolved in bovine serum affects the rheological properties of polymer mixture solution. The viscosity is directly related to the alginate concentration, and inversely related to the temperature[61,62]. In fact, the development of shape with high viscosity material becomes very easy in printing; however, the energy that has to be subtracted from the scaffold and/or the time for the freezing phase has to be added.

To identify the region of interest, we created a digital model and the related digital bio-library able to control the manufacturing phases. This library requires thorough validation, to apply the same file for its development with the largest number of hard and soft materials.

For these reasons, the identification of macro-morphology resolution must be merged with the printing parameters lower limits. The FANNAM method includes four processes: 3D reconstruction cutting (3DRC), 3D fast freeze gelation (3DFFG), nano

dry formulation (NDF), and 3D partial processes (3DPP), designing new digital elaboration steps to define the best correlation between different materials and technology. The final goal is the definition of an optimal printing configuration, and an alginate-based material formulation with integrated NP, while simultaneously disinfecting the 3D-printed object[43]. By using 3DRC, the missing biological components can be rebuilt, defining the best fit between the 3D model and the final trajectory related to printing materials[10]. The alginate-based materials with embedded NP we used for these experiments were made with NDF, without NP waste and with the goal to guarantee low variance in terms of released nano-laden material. We implemented 3DFFG, which allows fast gelation, the rapid release of alginate (approximately 2-3 minutes), and simultaneous disinfection, enabling the long-term preservation without any additional treatment[63]. In fact, once the adherent printed object is obtained with the digital model, the instantaneous gelation closed the loop for scaffold fabrication, fixing the freezed scaffold promptly.

The functional adherence of the 3D-printed object, the amount of used material, and the similarity with the digital model are assured via the 3DPP. 3DPP includes all activities of configuration, calibration or modification carried out in the processes and stages of 3D model development, which competes for maximum quality performance. Partial processes are therefore mandatory in the development of 3D-printed objects through rapid prototyping and viscous materials. For instance, if we change the development speed on a machine with a subtractive technology, the surface roughness alteration does not modify the mechanical characteristics; on the other hand, when using the additive manufacturing technology to realise cake decorations, its morphology changes, obtaining the functional aim of the object (aesthetics, in this case). Thus, the assessment of the parameters is directly related with the functionality of the 5D object,

and in the case of soft tissue realization, we must take into account accidentally falling drops, or the creation of vascular channel to bring, where required, the gelation fluid for the morphology long-term fixation. Dedicated tests are required to better assess any manufactured object and each possible customisation[61,62,64–68].

Eventually, post-print and analyses increase the quality and the biological potentials of digitalised pathological models and the evaluation of the printed 5D model adherence, assuring a continuous improvement system with the use of a custom CATE for the smart and fast storing of all processed data in new digital library pathology[10].

In virtue of the high scaffold customisation potential (NP or functionalised matrix for a gradual drug release), we can design and bio-print 5D personalised medical devices. Specifically, by modifying the composite biomaterial and the manufacturing methods, the interaction of the grafted structures with the biological substrate may be modified in accordance with the experimental requirements[69–71]. When it is possible to transplant bio-compatible tissues (prosthetic grafts, stents, etc.) and activate the functionalised material for restoring physiological activity (with, for instance, external stimuli such as electrical, magnetic, photonic, etc., or chemical agents), the 5D printing becomes "active"[41,72]. Therefore, as a result of the analyses and the digitalisation of the diseases over time, it is possible to validate and determine key directives in order to develop the region of interest for the scaffolds for future *in-vivo tests*.

The method we described can be applied to different types of materials and gelation. In this study, we used alginate, and gelled the scaffold with EtOH and $CaCl_2$. These two developed bio-materials scaffolds demonstrated distinctive micro-morphology as well as functional application. Anyway, both of these bio-materials were associated with a low influence on cell viability. These developed devices demonstrated the capability to control gradual release, as we confirmed with our *in-vitro* and *in-vivo*

studies regarding dissolution of the 5D-printed device in a solution with VSMC and, consequently, in an albino rat's inferior vena cava. The pharmacokinetics and pharmacodynamics of the release was very similar to DCB application. Moreover, these nano-laden scaffolds demonstrated to be able to carry NP, and also their long-term storage potential was confirmed. Reproducing the same tests on HUVEC, the results demonstrated the potential of human scaling of the proposed method. The high variability in biological application requires rigorous standards for analysis and we identified a good scheduling for the 5D processes and parameters digitalisation with the goal to support the synthetic organ development and the digital bio-library improvement. Our method showed that is possible to develop nano-laden 5D devices for training, pharmacological tests and *in-vivo* applications, and the possibility to improve the current DCB therapy, merging patients morphology with the high resolution of RFP technology.

Conclusions

3D-printing of a custom balloon coating is feasible. These printed scaffolds with 11% of alginate concentration demonstrated no toxicity in *in-vitro* studies. These biocompatible scaffolds can be integrated with active NP, and their effectiveness was confirmed in both *in-vitro* and *in-vivo* tests (NP internalisation in target cells and tissues). This method paves the way for future personalised medicine, since these 5D-printed scaffolds can be functionalized with different nanoparticles, i.e. fluorescent nano-beads as a convenient model of drug carrier, chemo-carrying nanoparticles (e.g. paclitaxel), or plasmonic nanoparticles.

References

1.   Adam DJ, Beard JD, Cleveland T, Bell J, Bradbury AW, Forbes JF, et al. Bypass versus angioplasty in severe ischaemia of the leg (BASIL): multicentre, randomised controlled trial. Lancet Lond Engl. 2005 Dec 3;366(9501):1925–34.

2.   Schneider PA, Laird JR, Tepe G, Brodmann M, Zeller T, Scheinert D, et al. Treatment Effect of Drug-Coated Balloons Is Durable to 3 Years in the Femoropopliteal Arteries: Long-Term Results of the IN.PACT SFA Randomized Trial. Circ Cardiovasc Interv. 2018;11(1):e005891.

3.   Kang H-W, Lee SJ, Ko IK, Kengla C, Yoo JJ, Atala A. A 3D bioprinting system to produce human-scale tissue constructs with structural integrity. Nat Biotechnol. 2016 Mar;34(3):312–9.

4.   Wang L, Xu M-E, Luo L, Zhou Y, Si P. Iterative feedback bio-printing-derived cell-laden hydrogel scaffolds with optimal geometrical fidelity and cellular controllability. Sci Rep. 2018 12;8(1):2802.

5.   Hunt NC, Grover LM. Cell encapsulation using biopolymer gels for regenerative medicine. Biotechnol Lett. 2010 Jun;32(6):733–42.

6.   Spiller KL, Maher SA, Lowman AM. Hydrogels for the repair of articular cartilage defects. Tissue Eng Part B Rev. 2011 Aug;17(4):281–99.

7.   Li Z, Kawashita M. Current progress in inorganic artificial biomaterials. J Artif Organs Off J Jpn Soc Artif Organs. 2011 Sep;14(3):163–70.

8.   Elviri L, Foresti R, Bianchera A, Silvestri M, Bettini R. 3D-printed polylactic acid supports for enhanced ionization efficiency in desorption electrospray mass spectrometry analysis of liquid and gel samples. Talanta. 2016 01;155:321–8.

9.   Gillaspie EA, Matsumoto JS, Morris NE, Downey RJ, Shen KR, Allen MS, et al. From 3-Dimensional Printing to 5-Dimensional Printing: Enhancing Thoracic

Surgical Planning and Resection of Complex Tumors. Ann Thorac Surg. 2016 May;101(5):1958–62.

10.   Foresti R, Rossi S, Pinelli S, Alinovi R, Sciancalepore C, Delmonte N, et al. In-vivo vascular application via ultra-fast bioprinting for future 5D personalised nanomedicine. Sci Rep. 2020 21;10(1):3205.

11.   Patel RAG, Sakhuja R, White CJ. The Medical and Endovascular Treatment of PAD: A Review of the Guidelines and Pivotal Clinical Trials. Curr Probl Cardiol. 2020 Jul;45(7):100402.

12.   Antithrombotic Trialists' Collaboration. Collaborative meta-analysis of randomised trials of antiplatelet therapy for prevention of death, myocardial infarction, and stroke in high risk patients. BMJ. 2002 Jan 12;324(7329):71–86.

13.   Tangelder MJ, Lawson JA, Algra A, Eikelboom BC. Systematic review of randomized controlled trials of aspirin and oral anticoagulants in the prevention of graft occlusion and ischemic events after infrainguinal bypass surgery. J Vasc Surg. 1999 Oct;30(4):701–9.

14.   Anand SS, Caron F, Eikelboom JW, Bosch J, Dyal L, Aboyans V, et al. Major Adverse Limb Events and Mortality in Patients With Peripheral Artery Disease: The COMPASS Trial. J Am Coll Cardiol. 2018 22;71(20):2306–15.

15.   Aboyans V, Ricco J-B, Bartelink M-LEL, Björck M, Brodmann M, Cohnert T, et al. Editor's Choice - 2017 ESC Guidelines on the Diagnosis and Treatment of Peripheral Arterial Diseases, in collaboration with the European Society for Vascular Surgery (ESVS). Eur J Vasc Endovasc Surg Off J Eur Soc Vasc Surg. 2018;55(3):305–68.

16.   Antoniou GA, Fisher RK, Georgiadis GS, Antoniou SA, Torella F. Statin therapy in lower limb peripheral arterial disease: Systematic review and meta-analysis.

Vascul Pharmacol. 2014 Nov;63(2):79–87.

17.   Westin GG, Armstrong EJ, Bang H, Yeo K-K, Anderson D, Dawson DL, et al. Association between statin medications and mortality, major adverse cardiovascular event, and amputation-free survival in patients with critical limb ischemia. J Am Coll Cardiol. 2014 Feb 25;63(7):682–90.

18.   Conte MS, Bradbury AW, Kolh P, White JV, Dick F, Fitridge R, et al. Global Vascular Guidelines on the Management of Chronic Limb-Threatening Ischemia. Eur J Vasc Endovasc Surg Off J Eur Soc Vasc Surg. 2019;58(1S):S1-S109.e33.

19.   Lane R, Ellis B, Watson L, Leng GC. Exercise for intermittent claudication. Cochrane Database Syst Rev. 2014 Jul 18;(7):CD000990.

20.   Society for Vascular Surgery Lower Extremity Guidelines Writing Group, Conte MS, Pomposelli FB, Clair DG, Geraghty PJ, McKinsey JF, et al. Society for Vascular Surgery practice guidelines for atherosclerotic occlusive disease of the lower extremities: management of asymptomatic disease and claudication. J Vasc Surg. 2015 Mar;61(3 Suppl):2S-41S.

21.   Mills JL, Conte MS, Armstrong DG, Pomposelli FB, Schanzer A, Sidawy AN, et al. The Society for Vascular Surgery Lower Extremity Threatened Limb Classification System: risk stratification based on wound, ischemia, and foot infection (WIfI). J Vasc Surg. 2014 Jan;59(1):220-234.e1-2.

22.   Norgren L, Hiatt WR, Dormandy JA, Nehler MR, Harris KA, Fowkes FGR, et al. Inter-Society Consensus for the Management of Peripheral Arterial Disease (TASC II). J Vasc Surg. 2007 Jan;45 Suppl S:S5-67.

23.   Pereira CE, Albers M, Romiti M, Brochado-Neto FC, Pereira CAB. Meta-analysis of femoropopliteal bypass grafts for lower extremity arterial

insufficiency. J Vasc Surg. 2006 Sep;44(3):510–7.

24.   Changal KH, Syed MA, Dar T, Mangi MA, Sheikh MA. Systematic Review and Proportional Meta-Analysis of Endarterectomy and Endovascular Therapy with Routine or Selective Stenting for Common Femoral Artery Atherosclerotic Disease. J Intervent Cardiol. 2019;2019:1593401.

25.   DeCarlo C, Boitano LT, Sumpio B, Latz CA, Feldman Z, Pendleton AA, et al. Comparative Analysis of Outcomes in Patients Undergoing Femoral Endarterectomy plus Endovascular (Hybrid) or Bypass for Femoropopliteal Occlusive Disease. Ann Vasc Surg. 2020 Sep 11;

26.   Indes JE, Pfaff MJ, Farrokhyar F, Brown H, Hashim P, Cheung K, et al. Clinical outcomes of 5358 patients undergoing direct open bypass or endovascular treatment for aortoiliac occlusive disease: a systematic review and meta-analysis. J Endovasc Ther Off J Int Soc Endovasc Spec. 2013 Aug;20(4):443–55.

27.   Bisdas T, Borowski M, Stavroulakis K, Torsello G, CRITISCH Collaborators. Endovascular Therapy Versus Bypass Surgery as First-Line Treatment Strategies for Critical Limb Ischemia: Results of the Interim Analysis of the CRITISCH Registry. JACC Cardiovasc Interv. 2016 26;9(24):2557–65.

28.   Dinh K, Gomes ML, Thomas SD, Paravastu SCV, Holden A, Schneider PA, et al. Mortality After Paclitaxel-Coated Device Use in Patients With Chronic Limb-Threatening Ischemia: A Systematic Review and Meta-Analysis of Randomized Controlled Trials. J Endovasc Ther Off J Int Soc Endovasc Spec. 2020;27(2):175–85.

29.   Wardle BG, Ambler GK, Radwan RW, Hinchliffe RJ, Twine CP. Atherectomy for peripheral arterial disease. Cochrane Database Syst Rev. 2020 29;9:CD006680.

30.   Ipema J, Huizing E, Schreve MA, de Vries J-PPM, Ünlü Ç. Editor's

Choice - Drug Coated Balloon Angioplasty vs. Standard Percutaneous Transluminal Angioplasty in Below the Knee Peripheral Arterial Disease: A Systematic Review and Meta-Analysis. Eur J Vasc Endovasc Surg Off J Eur Soc Vasc Surg. 2020;59(2):265–75.

31.   Veenstra EB, van der Laan MJ, Zeebregts CJ, de Heide E-J, Kater M, Bokkers RPH. A systematic review and meta-analysis of endovascular and surgical revascularization techniques in acute limb ischemia. J Vasc Surg. 2020;71(2):654-668.e3.

32.   Dey M, Ozbolat IT. 3D bioprinting of cells, tissues and organs. Sci Rep. 2020 Aug 18;10(1):14023.

33.   Hospodiuk M, Dey M, Sosnoski D, Ozbolat IT. The bioink: A comprehensive review on bioprintable materials. Biotechnol Adv. 2017 Apr;35(2):217–39.

34.   Ozbolat IT, Hospodiuk M. Current advances and future perspectives in extrusion-based bioprinting. Biomaterials. 2016 Jan;76:321–43.

35.   Gudapati H, Dey M, Ozbolat I. A comprehensive review on droplet-based bioprinting: Past, present and future. Biomaterials. 2016;102:20–42.

36.   Kim IG, Park SA, Lee S-H, Choi JS, Cho H, Lee SJ, et al. Transplantation of a 3D-printed tracheal graft combined with iPS cell-derived MSCs and chondrocytes. Sci Rep. 2020 09;10(1):4326.

37.   Barbeck M, Serra T, Booms P, Stojanovic S, Najman S, Engel E, et al. Analysis of the in vitro degradation and the in vivo tissue response to bi-layered 3D-printed scaffolds combining PLA and biphasic PLA/bioglass components - Guidance of the inflammatory response as basis for osteochondral regeneration. Bioact Mater. 2017 Dec;2(4):208–23.

38.   Rutala WA, Weber DJ. New disinfection and sterilization methods. Emerg Infect Dis. 2001 Apr;7(2):348–53.

39.   Rossi S, Savi M, Mazzola M, Pinelli S, Alinovi R, Gennaccaro L, et al. Subchronic exposure to titanium dioxide nanoparticles modifies cardiac structure and performance in spontaneously hypertensive rats. Part Fibre Toxicol. 2019 24;16(1):25.

40.   Miragoli M, Ceriotti P, Iafisco M, Vacchiano M, Salvarani N, Alogna A, et al. Inhalation of peptide-loaded nanoparticles improves heart failure. Sci Transl Med. 2018 17;10(424).

41.   Kokkinis D, Schaffner M, Studart AR. Multimaterial magnetically assisted 3D printing of composite materials. Nat Commun. 2015 Oct 23;6:8643.

42.   Ravnic DJ, Leberfinger AN, Koduru SV, Hospodiuk M, Moncal KK, Datta P, et al. Transplantation of Bioprinted Tissues and Organs: Technical and Clinical Challenges and Future Perspectives. Ann Surg. 2017;266(1):48–58.

43.   Lee JM, Sing SL, Zhou M, Yeong WY. 3D bioprinting processes: A perspective on classification and terminology. Int J Bioprinting [Internet]. 2018 Jul 3 [cited 2020 Oct 2];4(2). Available from: http://ijb.whioce.com/index.php/int-j-bioprinting/article/view/151

44.   Gurikov P, Smirnova I. Non-Conventional Methods for Gelation of Alginate. Gels Basel Switz. 2018 Feb 1;4(1).

45.   Hajal C, Campisi M, Mattu C, Chiono V, Kamm RD. In vitro models of molecular and nano-particle transport across the blood-brain barrier. Biomicrofluidics. 2018 Jul;12(4):042213.

46.   Fowkes FGR, Rudan D, Rudan I, Aboyans V, Denenberg JO, McDermott MM, et al. Comparison of global estimates of prevalence and risk factors for peripheral artery disease in 2000 and 2010: a systematic review and analysis. Lancet

Lond Engl. 2013 Oct 19;382(9901):1329–40.

47.   Sanna G, Alesso D, Mediati M, Cimminiello C, Borghi C, Fazzari AL, et al. Prevalence of peripheral arterial disease in subjects with moderate cardiovascular risk: Italian results from the PANDORA study Data from PANDORA (Prevalence of peripheral Arterial disease in subjects with moderate CVD risk, with No overt vascular Diseases nor Diabetes mellitus). BMC Cardiovasc Disord. 2011 Oct 7;11:59.

48.   Bunte MC, Shishehbor MH. Next Generation Endovascular Therapies in Peripheral Artery Disease. Prog Cardiovasc Dis. 2018 Apr;60(6):593–9.

49.   Schillinger M, Sabeti S, Loewe C, Dick P, Amighi J, Mlekusch W, et al. Balloon angioplasty versus implantation of nitinol stents in the superficial femoral artery. N Engl J Med. 2006 May 4;354(18):1879–88.

50.   Laird JR, Katzen BT, Scheinert D, Lammer J, Carpenter J, Buchbinder M, et al. Nitinol stent implantation vs. balloon angioplasty for lesions in the superficial femoral and proximal popliteal arteries of patients with claudication: three-year follow-up from the RESILIENT randomized trial. J Endovasc Ther Off J Int Soc Endovasc Spec. 2012 Feb;19(1):1–9.

51.   Krishnan P, Faries P, Niazi K, Jain A, Sachar R, Bachinsky WB, et al. Stellarex Drug-Coated Balloon for Treatment of Femoropopliteal Disease: Twelve-Month Outcomes From the Randomized ILLUMENATE Pivotal and Pharmacokinetic Studies. Circulation. 2017 Sep 19;136(12):1102–13.

52.   Rosenfield K, Jaff MR, White CJ, Rocha-Singh K, Mena-Hurtado C, Metzger DC, et al. Trial of a Paclitaxel-Coated Balloon for Femoropopliteal Artery Disease. N Engl J Med. 2015 Jul 9;373(2):145–53.

53.   Dake MD, Ansel GM, Jaff MR, Ohki T, Saxon RR, Smouse HB, et al. Durable Clinical Effectiveness With Paclitaxel-Eluting Stents in the Femoropopliteal

Artery: 5-Year Results of the Zilver PTX Randomized Trial. Circulation. 2016 Apr 12;133(15):1472–83; discussion 1483.

54. Murphy SV, Atala A. 3D bioprinting of tissues and organs. Nat Biotechnol. 2014 Aug;32(8):773–85.

55. Hong N, Yang G-H, Lee J, Kim G. 3D bioprinting and its in vivo applications. J Biomed Mater Res B Appl Biomater. 2018 Jan;106(1):444–59.

56. Hodgdon T, Danrad R, Patel MJ, Smith SE, Richardson ML, Ballard DH, et al. Logistics of Three-dimensional Printing: Primer for Radiologists. Acad Radiol. 2018 Jan;25(1):40–51.

57. He Y, Yang F, Zhao H, Gao Q, Xia B, Fu J. Research on the printability of hydrogels in 3D bioprinting. Sci Rep. 2016 20;6:29977.

58. Elviri L, Foresti R, Bergonzi C, Zimetti F, Marchi C, Bianchera A, et al. Highly defined 3D printed chitosan scaffolds featuring improved cell growth. Biomed Mater Bristol Engl. 2017 Jul 12;12(4):045009.

59. Shah P, Racasan R, Bills P. Comparison of different additive manufacturing methods using computed tomography. Case Stud Nondestruct Test Eval. 2016 Nov 1;6:69–78.

60. Tan Z, Parisi C, Di Silvio L, Dini D, Forte AE. Cryogenic 3D Printing of Super Soft Hydrogels. Sci Rep. 2017 24;7(1):16293.

61. Xu X, Han Q, Shi J, Zhang H, Wang Y. Structural, thermal and rheological characterization of bovine serum albumin binding with sodium alginate. J Mol Liq. 2020 Feb 1;299:112123.

62. Ma J, Lin Y, Chen X, Zhao B, Zhang J. Flow behavior, thixotropy and dynamical viscoelasticity of sodium alginate aqueous solutions. Food Hydrocoll. 2014 Jul 1;38:119–28.

63.   Ribeiro MM, Neumann VA, Padoveze MC, Graziano KU. Efficacy and effectiveness of alcohol in the disinfection of semi-critical materials: a systematic review. Rev Lat Am Enfermagem. 2015 Aug;23(4):741–52.

64.   Hashemnejad SM, Kundu S. Rheological properties and failure of alginate hydrogels with ionic and covalent crosslinks. Soft Matter. 2019 Oct 9;15(39):7852–62.

65.   Fernández Farrés I, Norton IT. Formation kinetics and rheology of alginate fluid gels produced by in-situ calcium release. Food Hydrocoll. 2014 Oct 1;40:76–84.

66.   Mahdi MH, Diryak R, Kontogiorgos V, Morris GA, Smith AM. In situ rheological measurements of the external gelation of alginate. Food Hydrocoll. 2016 Apr 1;55:77–80.

67.   Grandgirard J, Poinsot D, Krespi L, Nénon J-P, Cortesero A-M. Costs of secondary parasitism in the facultative hyperparasitoid Pachycrepoideus dubius: does host size matter? Entomol Exp Appl. 2002;103(3):239–48.

68.   Zhong D, Huang X, Yang H, Cheng R. New insights into viscosity abnormality of sodium alginate aqueous solution. Carbohydr Polym. 2010 Jul 23;81(4):948–52.

69.   Campisi M, Shin Y, Osaki T, Hajal C, Chiono V, Kamm RD. 3D self-organized microvascular model of the human blood-brain barrier with endothelial cells, pericytes and astrocytes. Biomaterials. 2018;180:117–29.

70.   Ronca A, Guarino V, Raucci MG, Salamanna F, Martini L, Zeppetelli S, et al. Large defect-tailored composite scaffolds for in vivo bone regeneration. J Biomater Appl. 2014 Nov;29(5):715–27.

71.   Serrano-Bello J, Cruz-Maya I, Suaste-Olmos F, González-Alva P,

Altobelli R, Ambrosio L, et al. In vivo Regeneration of Mineralized Bone Tissue in Anisotropic Biomimetic Sponges. Front Bioeng Biotechnol. 2020;8:587.

72.   Raviv D, Zhao W, McKnelly C, Papadopoulou A, Kadambi A, Shi B, et al. Active printed materials for complex self-evolving deformations. Sci Rep. 2014 Dec 18;4:7422.

Tables

Method	Parameters	Operative processes	Printing phases	Organ Printing Phases
Parameters identification	Region of interest	Imaging acquisition (CT, MRI, PET)	Images processing sectioning and cell isolation	PRE-PRINTING
Materials selection	Process	Technological sizing based upon material properties	Formulation	
Technology assessment	Geometrical	CATE (computed aided tissue engineering) processing	Blueprint	
Pre-processing reconstruction	Printing	3D imaging digitalization and printing simulation	3DRC (3D reconstruction cutting) and digital bio-library related to the model	
3D Object processing	Chemical and Physical	Additive manufacturing and fixation	3DFFG (3D fast freeze gelation)	PRINTING
4D Functionalization	Functional and biomimicry	Definition of dynamic and active properties	NDF (nano dry formulation)	
5D Customization	Pathology and physiology	Health device development	3DPP (3D partial processes) and digital bio-library functional customisation	
Therapy	Predictive	Biological tests	Biomonitoring	POST-PRINTING
Synthetic organ transplantation	Health guideline	Clinical analysis	Treatment and validation	
Bio-based smart bioprinting	Adaptive	Smart processing	Human mimicry and autonomous regeneration	

Table I. The 3 phases involved in 5D printed devices development (from pre-processing reconstructions, to 5D customisation). In this Table (adapted from our preliminarily published work: Foresti R *et al*. In-vivo vascular application via ultra-fast bioprinting for future 5D personalised nanomedicine. Sci Rep 2020;10:3205), methods, parameters, and operative processes are described.
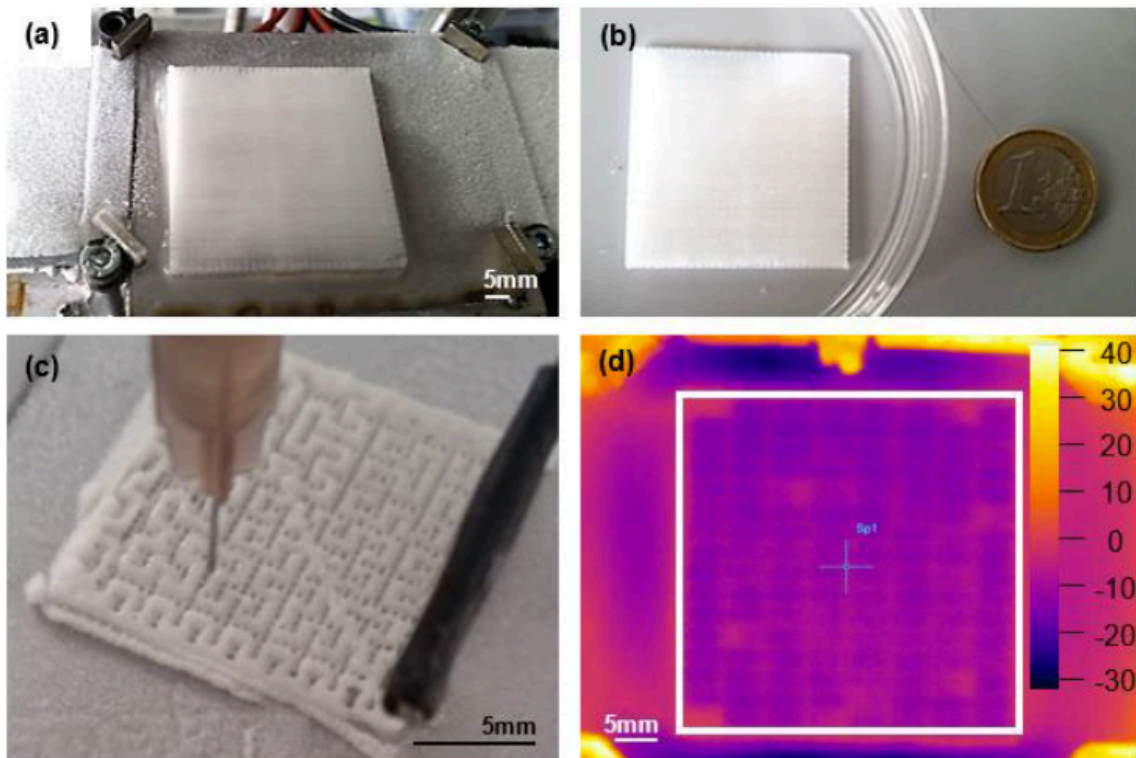
Figures

Figure 1. Peltier cold plate, and scaffold fabrication. (a) Bioscaffold with 200μm of macro-porosity on the Peltier cold plate. (b) Detail of the 47.5 x 47.5 mm 3D-printed scaffold. (c) Hybrid scaffold with Hilbert curve geometry. (d) Thermal camera visualization of the Peltier cell, and detail of electro-thermal transition. The white square identifies the analysed surface area.
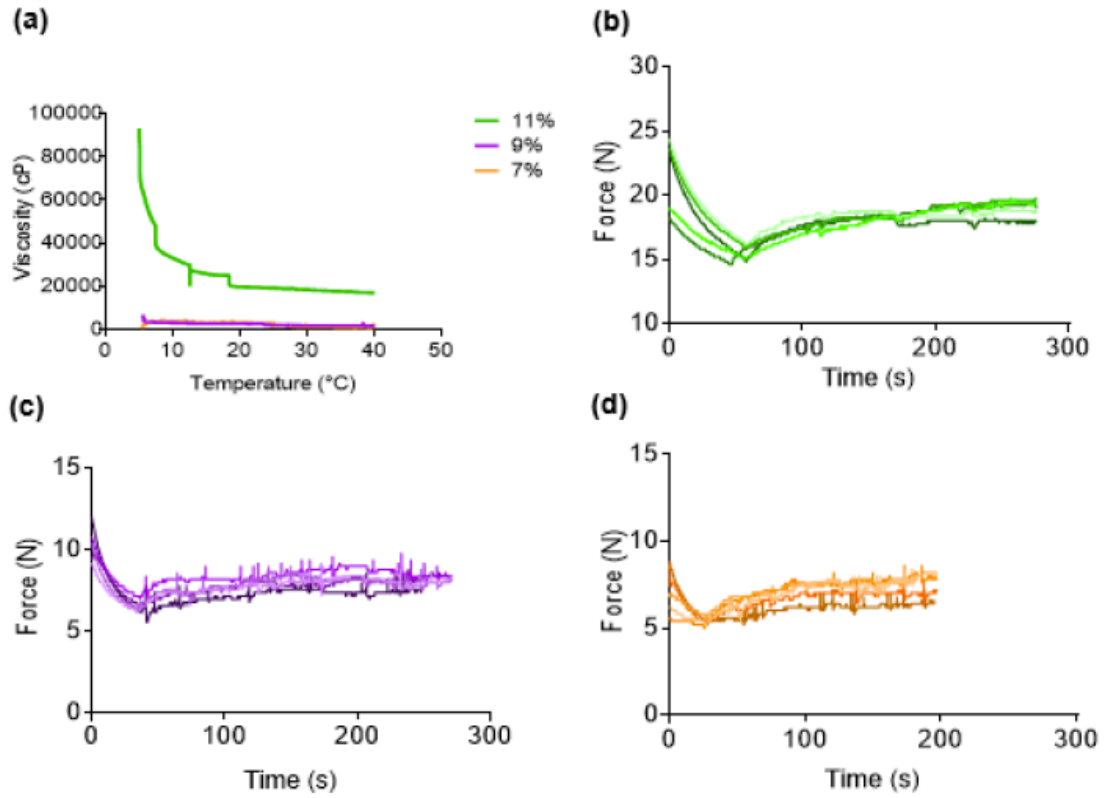
Figure 2. Viscosity and extrusion force applied to the syringe for three different alginate percentage scaffold fabrication. (a) Temperature/viscosity relation of different bio-ink alginate percentage (green: 11%; purple 9%; orange 7%). (b) Force applied to the syringe to print 5 different scaffolds with a speed of 20mm/s at 11% alginate concentration. (c) Force applied to the syringe to print 5 different scaffolds with a speed of 20mm/s at 9% alginate concentration. (d) Force applied to the syringe to print 5 different scaffolds with a speed of 20mm/s at 7% alginate concentration.
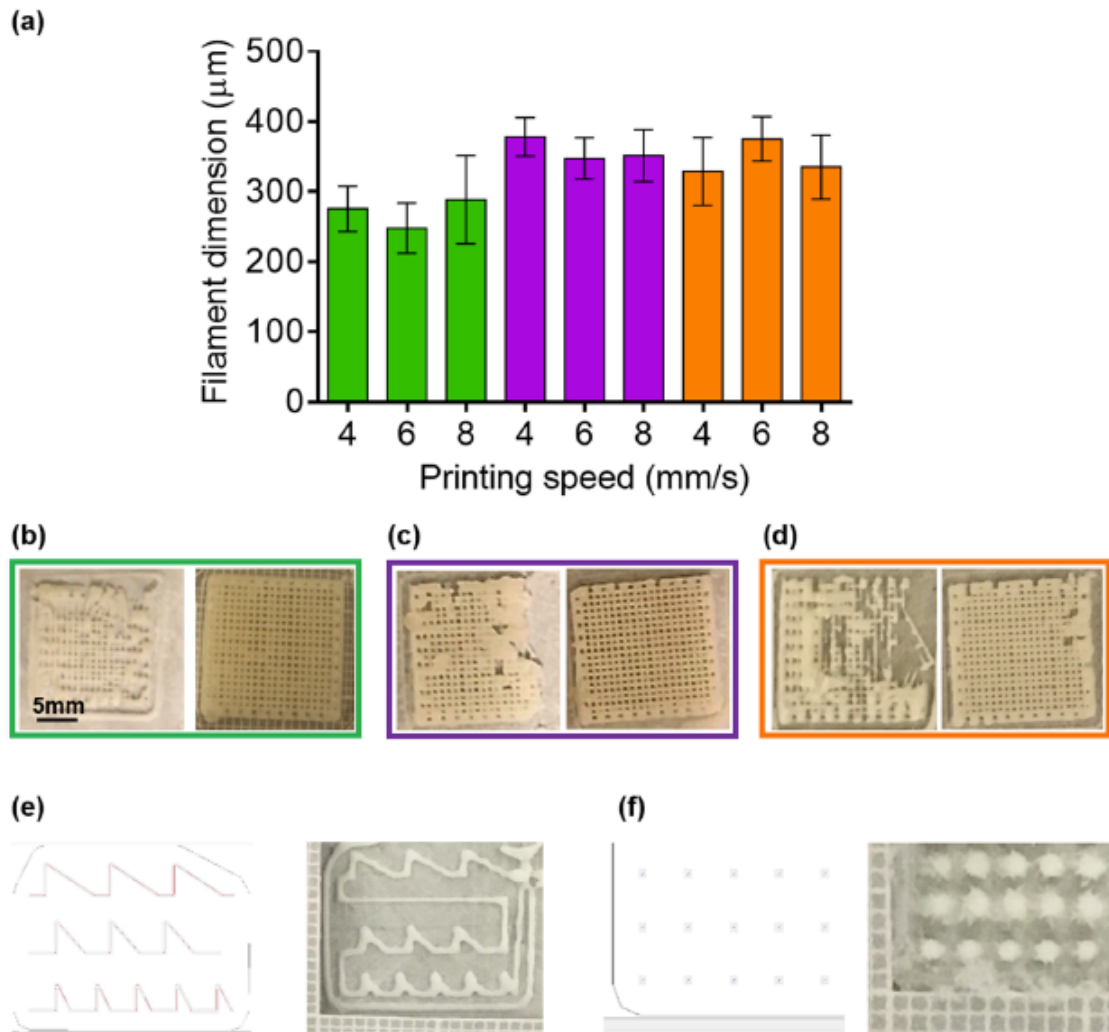
Figure 3. Scaffold macro-morphological characterisation and resolution assessment. (**a**) Scaffold filament diameter at different speed and alginate concentration with volume integration: 11% (green), 9% (purple), 7% (orange); (**b**) Printed scaffolds with 11% of alginate concentration under (left panel) and over (right panel) the minimum speed (6 mm/s). (**c**) same as (**b**) for printed scaffolds with 9% of alginate concentration and minimum speed of 10 mm/s. (**d**) same as (**b**) for printed scaffolds with 7% of alginate concentration and minimum speed of 14 mm/s. (**e**) Example of validation tests of printed corners at 60°, 45° and 30°: .STL file (left panel); printed trajectory (right panel). (**f**) Example of validation tests of printed drops: .STL file (left panel); printed trajectory (right panel). Wilcoxon sign rank test was performed and statistical significance was set at $p<.05$. Data are represented as median ± discrepancy. Note: adapted from our preliminarily published work Foresti R *et al*. Sci Rep 2020;10:3205.

46
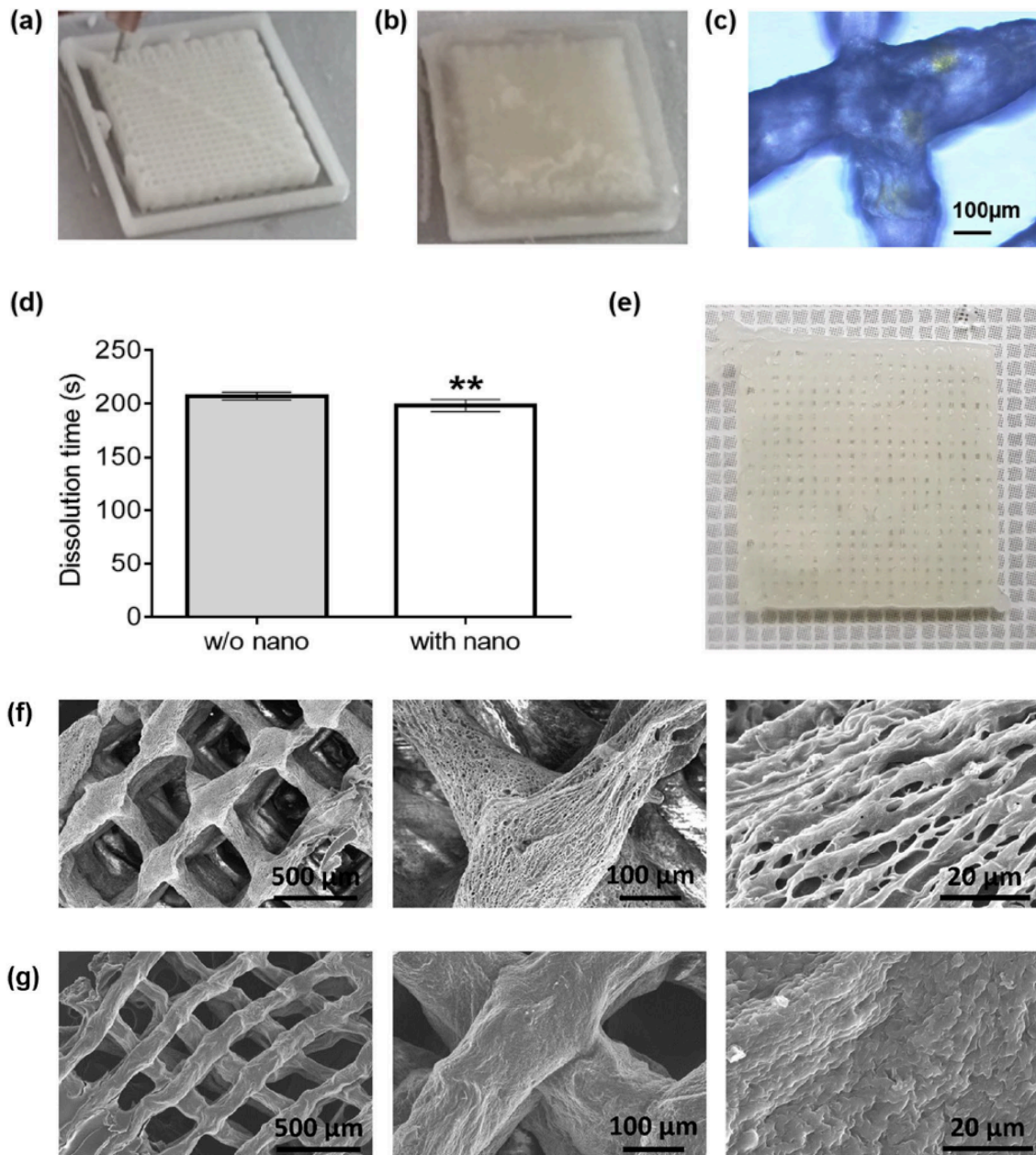
Figure 4. 3D Fast Freeze Gelation, dissolution time and micro-morphology. (**a**) Freeze fixation; (**b**) Freeze gelation; (**c**) Scaffold detail displaying fluorescence spots. (**d**) Dissolution time of alginate ethanol gelled scaffold in DMEM, without (grey), or with (white) nanoparticles. (**e**) Alginate based scaffold (gelled with $CaCl_2$) after 24 hours conservation in DMEM. (**f**) Alginate Scanning Electron Microscope (SEM) images of a 3D-printed scaffold gelled with $CaCl_2$, and with (**g**) ethanol at different magnifications. Unpaired t-test was performed and statistical significance was set at p<.05. ** with vs. without nanoparticles. Data are represented as mean ± SEM. Note: adapted from our preliminarily published work Foresti R *et al*. Sci Rep 2020;10:3205.
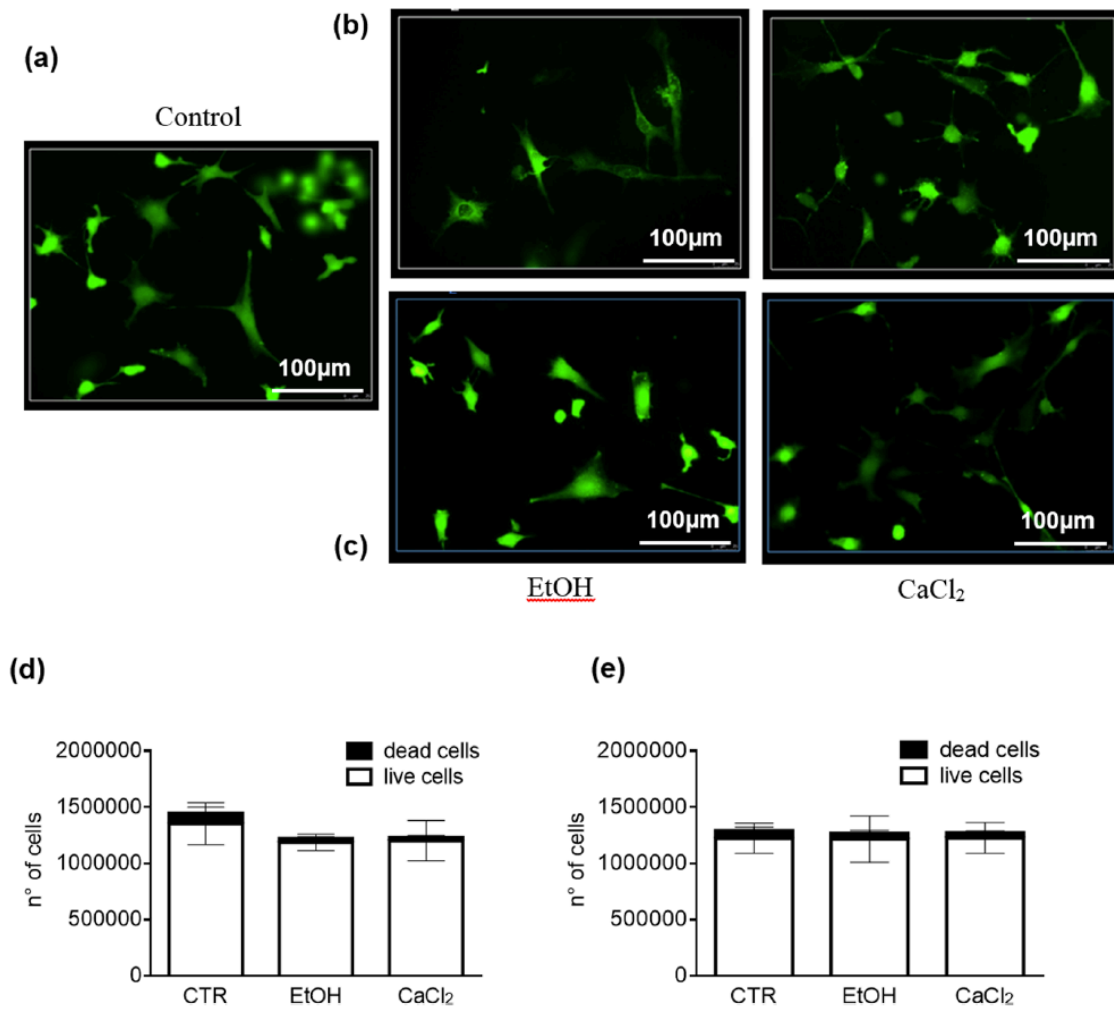
Figure 5. VSMC Viability. (**a**) Calcein AM-loaded VSMC after scaffold solubilisation with (**b**) direct or (**c**) indirect method gelled with EtOH (left panels) or CaCl$_2$ (right panels). VSMC viability (Live/Dead assay) after dissolving the scaffold gelled with EtOH or CaCl$_2$, with (**d**) direct or (**e**) indirect method. Unpaired t-test was performed and statistical significance was set at $p<.05$. Data are represented as mean ± SEM. Note: adapted from our preliminarily published work Foresti R *et al*. Sci Rep 2020;10:3205.
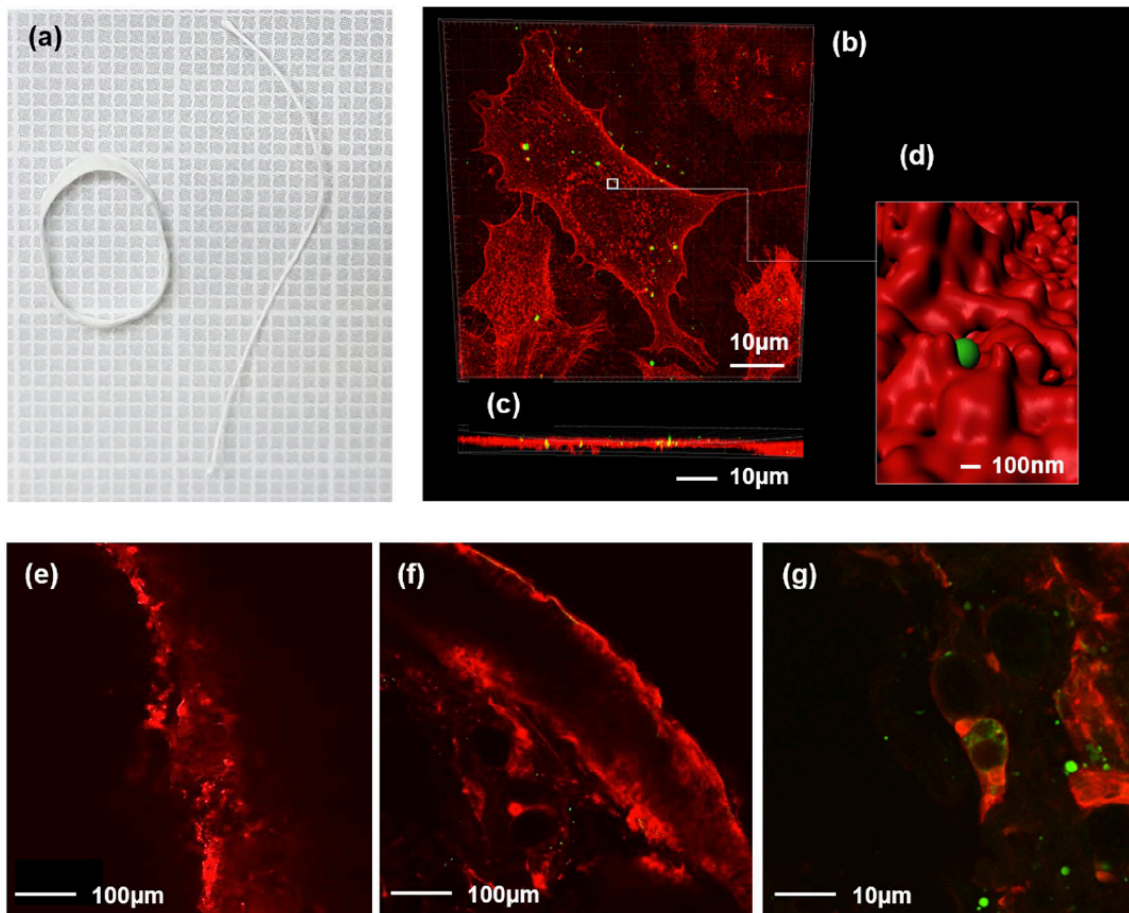
Figure 6. Scaffold-derived nanoparticles internalization. (**a**) Aerogel scaffold and filament after more than 12 months of storage in the petri dish. (**b**) Frontal view obtained by STED confocal microscopy of wheat germ agglutinin (WGA) stained vascular smooth muscle cells (VSMC, red) that included nanoparticles (green). (**c**) Orthogonal view showing the same nanoparticles into the cultured cells. (**d**) Render image obtained by the white square in "*b*" showing nanoparticle internalization from the VMSC membrane. Nanoparticle diameter: 40 nm. (**e**) Two-photon microscopy imaging of a WGA-stained rat vein. (**f**) Same as (**e**) with a vein exposed to the scaffold containing nanoparticles, showing the internalization of the nanoparticles in the VSMC cells. (**g**) same as (**f**) with high-scan resolution. Note: adapted from our preliminarily published work Foresti R *et al*. Sci Rep 2020;10:3205.
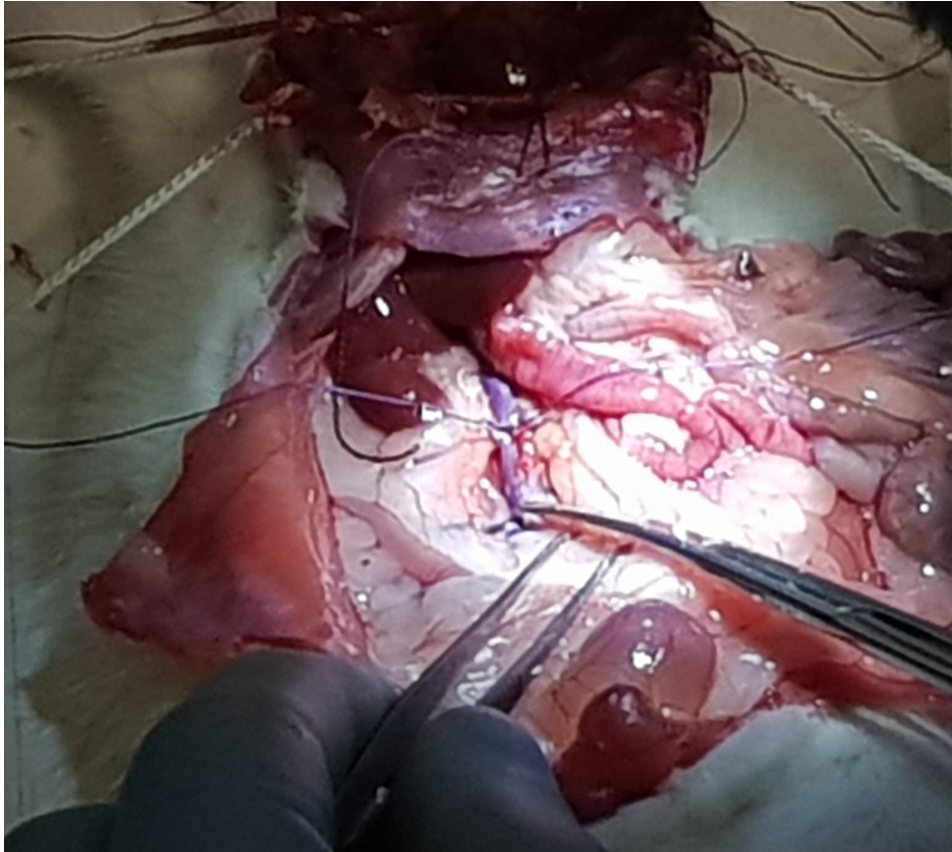
Figure 7. The rat's vena cava (purple structure in the middle of the picture) is isolated and ligated. We are preparing the venotomy (scissors), which will be used to insert the 3D-printed nano-laden filament for *in-vivo* analysis.
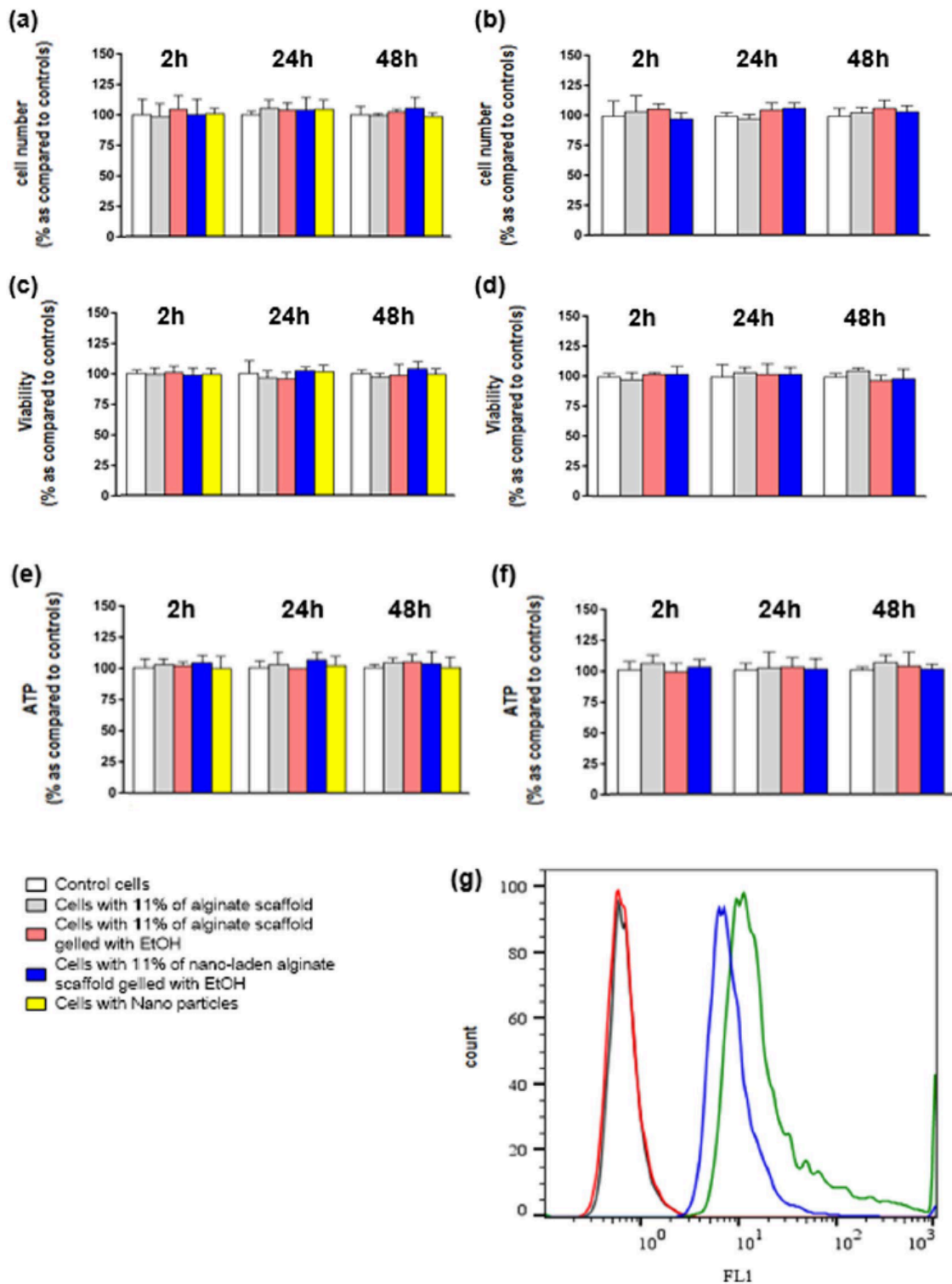
Figure 8. *In-vitro* viability and metabolism evaluation in HUVEC line (adapted from our preliminarily published work Foresti R *et al*. Sci Rep 2020;10:3205). (**a**) cell number evaluation at 2h, 24h and 48h after scaffold direct dissolution in: (i) control cell (first column); (ii) cells after 11% of alginate administration (second column); (iii) cell after 11% of alginate administration and ethanol crosslinking (third column); (iv) cell after 11% of alginate administration, ethanol crosslinking and NP

administration (forth column); (v) cell after NP administration (fifth column). (**b**) same as (**a**) for scaffold indirect dissolution. (**c**) cell viability evaluation at 2h, 24h and 48h after scaffold direct dissolution in: (i) control cell (first column); (ii) cells after 11% of alginate administration (second column); (iii) cell after 11% of alginate administration and ethanol crosslinking (third column); (iv) cell after 11% of alginate administration, ethanol crosslinking and NP administration (forth column); (v) cell after NP administration (fifth column). (**d**) same as (**c**) for scaffold indirect dissolution. (**e**) ATP evaluation at 2h, 24h and 48h after scaffold direct dissolution in: (i) control cell (first column); (ii) cells after 11% of alginate administration (second column); (iii) cell after 11% of alginate administration and ethanol crosslinking (third column); (iv) cell after 11% of alginate administration, ethanol crosslinking and NP administration (forth column); (v) cell after NP administration (fifth column). (**f**) same as (**e**) for scaffold indirect dissolution. White columns: control cells; grey columns: cells with 11% of alginate scaffold; pink columns: cells with 11% of alginate scaffold gelled with EtOH; blue columns: cells with 11% of alginate scaffold gelled with EtOH containing NPs: yellow columns: cells with NPs. (**g**) Cytofluorimetric analysis of HUVEC control cell after 24h (black trace), HUVEC and alginate after 24h (red trace), HUVEC and alginate plus NP after 2h (green trace) and after 24h (blue trace). Kruskal-Wallis (post hoc analyses: Dunn's multiple comparison) was performed and statistical significance was set at $p < .05$. Data are represented as mean ± SEM.
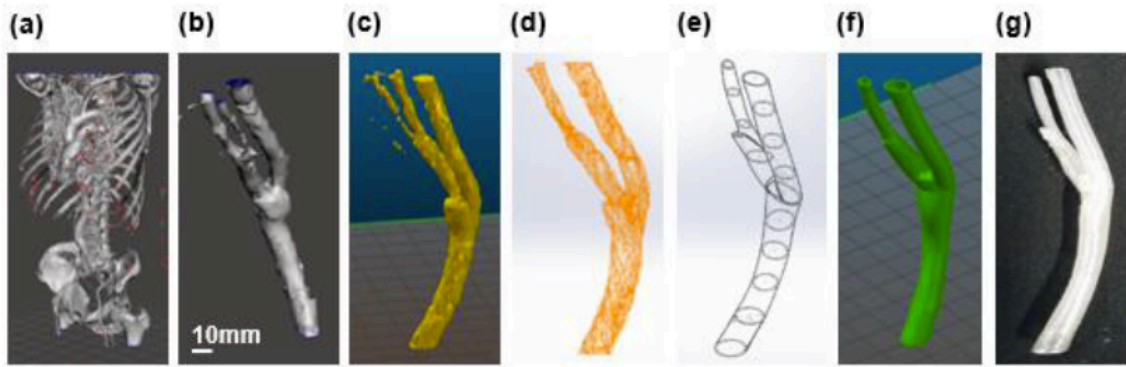
Figure 9. The process of 3D-printing starting from a CT-scan. (a) CT-angiography of the patient (3D Surface Rendering). (b) Cut section of the right femoral bifurcation. (c) The femoral bifurcation in .STL format. (d) Surfaces details of a non-printable .STL model. (e) 3D digital reconstructed model. (f) .STL format of a printable model. (g) The femoral bifurcation printed in polylactic acid.
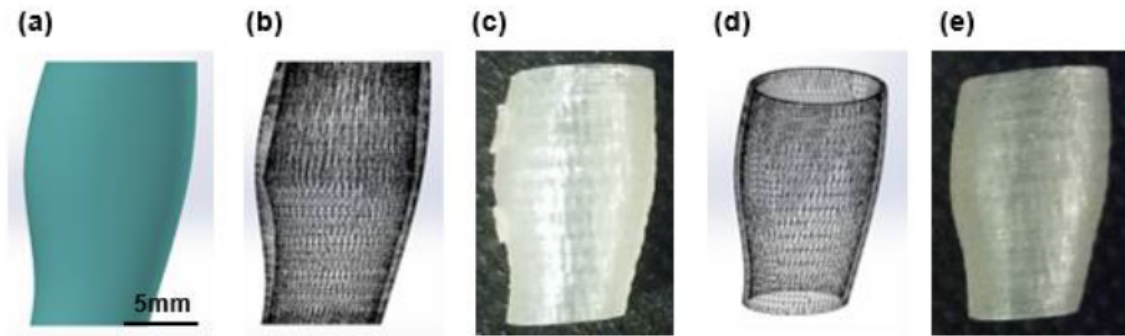
Figure 10. The 3D partial processes. (a) A section of a 3D-printed femoral artery. (b) Automatic .STL file generated by the CAD-like software. (c) 3D-printed PLA object, with defects. (d) Adapted and corrected .STL model. (e) 3D-printed object without defects, scalable and usable for tissue bioprinting.
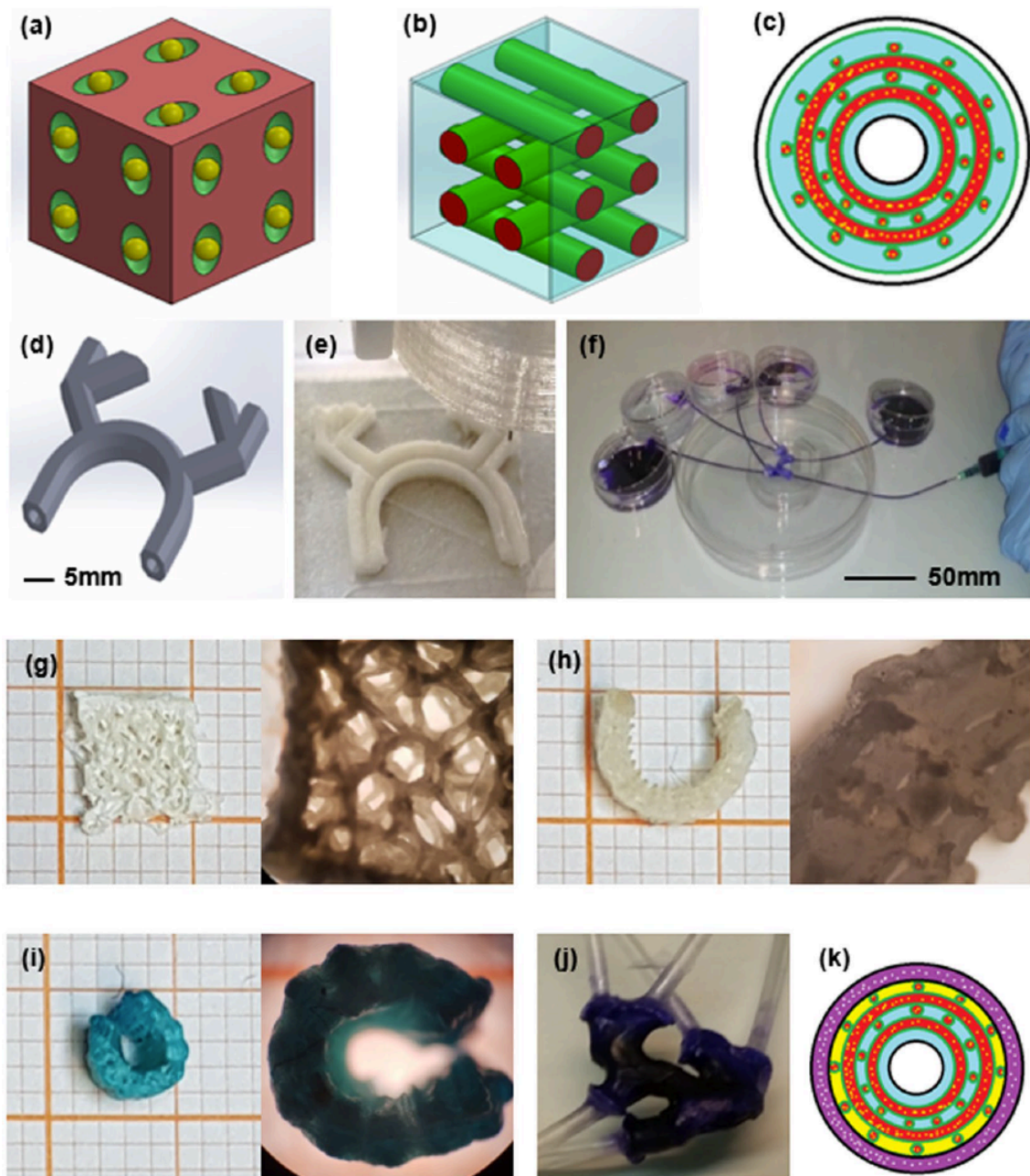
Figure 11. Bio-composite material vessel fabrication (adapted from our preliminarily published work Foresti R *et al*. Sci Rep 2020;10:3205). (**a**) Composite biomaterial (bio-based, biocompatible and biodegradable): matrix (red, functions), interface (green, performance and stability) and reinforcement (yellow, fibre, nanoparticles, nano-tubes, etc.). (**b**) Bio-composite material (Nano-functionalised 4D bio-engineered scaffold): matrix (blue, functions), interface (green, performance and stability) and fibre (red, composite/ biocomposite scaffold reinforcement). (**c**) Bio-composite material vessel schema: nano-laden fibre (yellow points and red), interface (green), not functionalised matrix (blue) and functionalised matrix (white). (**d**) 3D digital model of complex vessel. (**e**) Complex vessel section; (**f**) Nano-functionalised 4D Bio-engineered scaffold perfusion test. (**g**) Complex geometry aerogel scaffold (left panel) and related

detail (right panel, 4x magnification). (**h**) Aerogel with functionalised surface micro-porosity (left panel) and related detail (right panel, 4x magnification). (**i**) Nano-laden bioengineered scaffold (left panel) and related detail (right panel, 4x magnification). (**j**) Dehydrated 5D bioprinted vascular device after more than 24 months of Petri dish storage. (**k**) Bio-composite material customisation schema: nano-laden fibre (yellow points and red), interface (green), not functionalised matrix (blue), functionalised matrix for dedicated cells (yellow), adhesive coating (black) and customised matrix for physiology analyses (white point and violet).
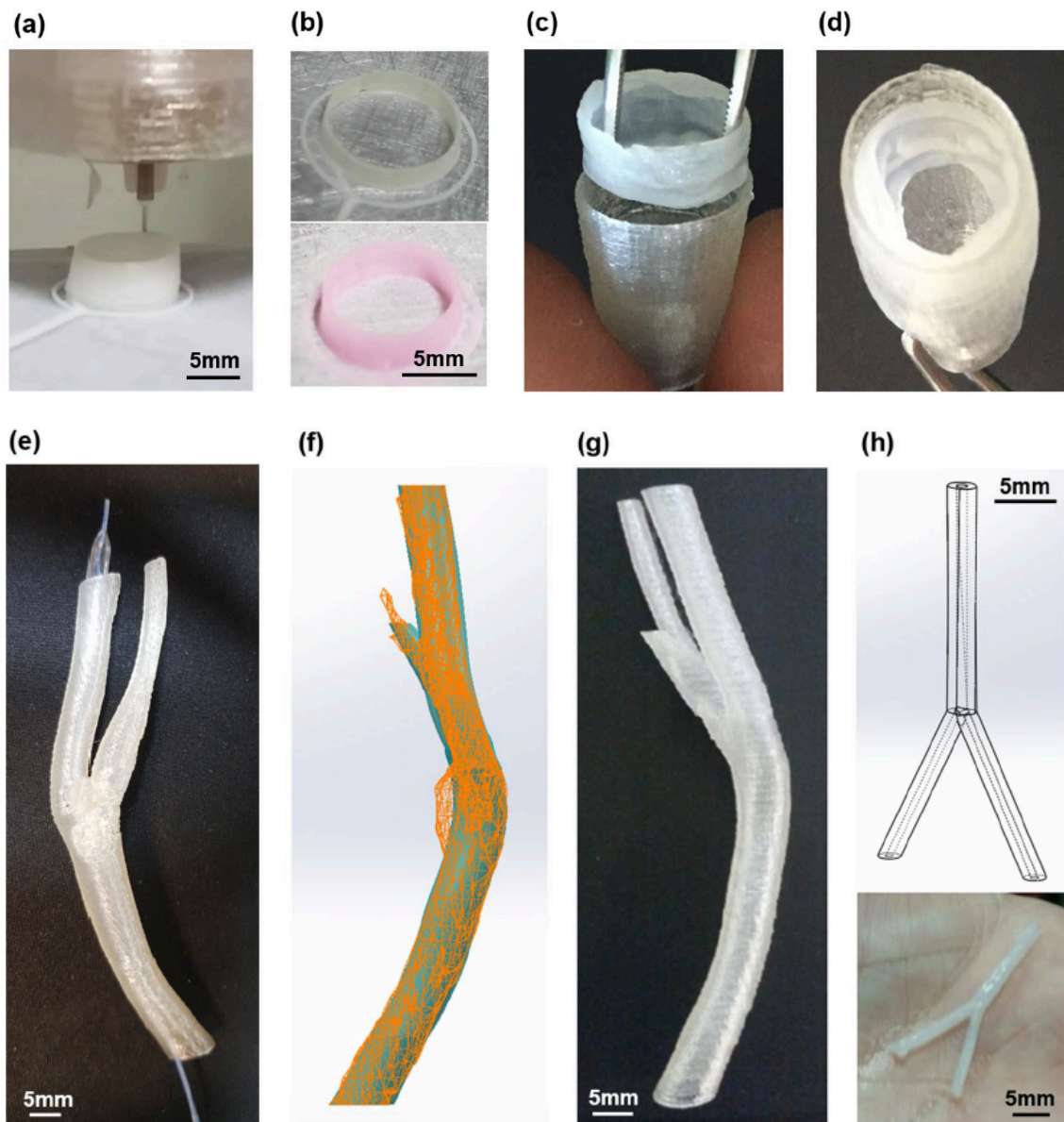
Figure 12. The 5D customised scaffold (adapted from our preliminarily published work Foresti R *et al*. Sci Rep 2020;10:3205). (**a**) 5D soft scaffold printing phase. (**b**) Composite biomaterial scaffold with green (upper panel) and red (lower panel) fluorescent nanoparticle. (**c** and **d**) Integration of soft and hard materials for gradual release tests. (**e**) Femoral bifurcation model for ballon angioplasty tests and training. (**f**) Surfaces detail of not printable .STL model with 3D digital reconstructed model. (**g**) 3D PLA printed model without pathology. (**h**) Capillary vascular bifurcation with 0.65 mm inner diameter and 1.7 mm outer diameter. Model design (upper panel), and 3D-printed object (lower panel).